Title: Partitioning environmental and philopatric drivers of nest site selection in an estuary-endemic turtle (*Malaclemys terrapin*)

Authors: Iwo P. Gross[1,2,*], Logan Register[3], & Matthew E. Wolak[1]

[1]Department of Biological Sciences, 120 W. Samford Avenue, Auburn University, Auburn, Alabama, 36849, USA

[2]Department of Biological Sciences, 116 St and 85 Ave, University of Alberta, Edmonton, Alberta, T6G 2R3, Canada

[3]Department of Biology, 902 14th Street South, University of Alabama at Birmingham, Birmingham, Alabama, 35205, USA

*Author for correspondence (E-mail: iwogross@gmail.com).

Running title: Spatially-explicit turtle nesting-habitat analysis

Acknowledgements

Jennifer DeBose, Jonathan Pitchford, and Kim Cressman at the Grand Bay National Estuarine Research Reserve graciously provided logistical support, and Dale Shirley and Charles Britt of the Chevron Pascagoula Refinery helped facilitate site access. Jon Armbruster and the Auburn University Museum of Natural History kindly provided the drone for our use, and Thane Wibbels of the University of Alabama at Birmingham provided access to Pix4D photogrammetric processing software. All study procedures were sanctioned under the AL Department of Conservation and Natural Resources permit numbers 2023122910268680 and 2023122911468680 and under the approved Auburn University Institutional Animal Care and Use Committee Protocol 2023-5273.

Conflict of interest

The authors declare no conflict of interest.

Statement of inclusion

Our study was conducted by a team of undergraduate, graduate, and faculty researchers from institutions in the region where the study was carried out. Active collaboration with reserve staff at Grand Bay National Estuarine Research Reserve supported data collection; these contributions are recognized in the acknowledgements. The project also provided training opportunities in drone-based mapping and spatial analysis for early-career researchers. We recognize that greater formal involvement of agency professionals as co-authors would further strengthen the regional embeddedness of this work and intend to prioritize these relationships in future projects.

Data availability

All data and R code are available from the Zenodo Digital Repository (https://doi.org/10.5281/zenodo.20116947).

Author contributions

Conceptualization: I.P.G. and M.E.W.; data curation: I.P.G. and L.R.; formal analysis: I.P.G. and M.E.W.; investigation: I.P.G.; project administration: M.E.W.; visualization: I.P.G. and L.R.; writing original manuscript: I.P.G.; writing – review and editing: L.R. and M.E.W.

Abstract

1. Oviposition site selection is a critical maternal effect with direct implications for population-level adaptation to environmental change. This process is driven by a complex interplay of environmental, density-dependent, and social factors whose relative contributions to site selection are rarely quantified simultaneously. Natal philopatry, for example, is a maternal effect that can direct oviposition site selection independently of local conditions, thus confounding estimates of adaptive habitat selection.

2. We conducted a spatially-explicit habitat selection analysis of oviposition sites in the diamond-backed terrapin (*Malaclemys terrapin*), a species in which nesting habitat selection and nesting site philopatry have been documented yet never evaluated within a unified statistical framework. We hypothesized that females select sites based on vegetation and topographic features that maximize offspring survival. We predicted these patterns would exhibit scale-dependence, and that selected conditions would promote hatching success.

3. We integrated resource selection functions with distance-based Moran's eigenvector maps and drone-derived three-dimensional habitat maps to analyze terrapin nest-habitat associations and partition variance in nest site selection among environmental features and residual spatial structure across multiple scales. This framework controls for bias due to spatial autocorrelation in nest occurrence data, quantifies scale-dependence of habitat selection, and partitions residual spatial variance consistent with latent social processes.

4. We found that terrapins selected vegetation complexity and elevation at broad spatial scales (1773 to 1927m), and terrain aspect at moderate scales (1192 to 1773m). The strength and direction of selection varied spatially across several habitat features, suggesting latent philopatric processes influence nest distributions independently of measured environmental gradients.

Furthermore, maternal selection for nest sites with vegetation and elevation values that predict reduced hatching success suggest a philopatric ecological trap in which maternally inherited site preferences have become decoupled from current habitat quality.

5. We demonstrate that environmental habitat quality alone cannot fully explain terrapin nest distributions, and that spatially-explicit variance partitioning can reveal latent philopatric signals in point-occurrence behavioral datasets when direct social observation is unavailable. These results highlight the importance of simultaneously modeling environmental and social drivers of maternal habitat selection, particularly as environmental change might decouple historically adaptive site use from environmental conditions.

Keywords: Diamondback terrapin; Parental effects; Photogrammetry; Site fidelity; Spatial eigenvector maps; Species distribution model; Testudines; UAV

Introduction

Maternal effects occur when females directly influence offspring traits through non-genetic mechanisms (Kirkpatrick & Lande, 1989), driving trait variation and shaping phenotypes in response to environmental heterogeneity (Mousseau & Fox, 1998). Maternal effects are often exemplified as parental care, such as food supplementation or lactation, physical defense, and protection from environmental exposure (Bernardo, 1996). Yet, in species which produce precocious offspring and lack true parental care, maternal selection for oviposition sites is considered a major maternal effect that can influence offspring survival and reproductive success (Resetarits, 1996), as well as the survivorship of ovipositing females (Refsnider & Janzen, 2010). Consequently, identifying the environmental variables that govern these decisions is vital to characterize the evolutionary implications of maternal effects and their influence on the trajectories of animal populations. However, the study of oviposition site selection is frequently complicated by latent social factors, such as density-dependent pressures (Ellis, 2008), conspecific attraction (Rudolf & Rödel, 2005), or natal philopatry (Weatherhead & Forbes, 1994), that potentially confound the influence of mechanistic habitat character choices.

These complications underscore a fundamental question in ecology: how do environmental and social processes interact to define organismal population densities and distributions? Habitat selection theory conceptualizes this complexity as a density-dependent pressure where conspecific densities modulate perceived site quality through resource depletion or territoriality (Fretwell & Lucas, 1969). Conversely, conspecific attraction or social signaling can stimulate gregarious behavior, such as when individuals use the presence of others as a cue for optimal habitat (Boström-Einarsson et al., 2025; Rushing et al., 2021). Natal philopatry represents a specific extension of these concepts in which maternal lineages culturally inherit

oviposition sites, often without direct contact among kin (Carreras et al., 2018; Freedberg et al., 2005; Reinhold, 1998). Because kin use sites asynchronously and across generations, this behavior is difficult to quantify without genetic techniques or long-term demographic sampling (Weatherhead & Forbes, 1994). Ultimately, uncertainty regarding the drivers of site choice in philopatric species prevents the effective partitioning of environmental versus cultural maternal effects and their influence on fitness.

Accurately attributing space use to mechanistic habitat preferences versus latent social processes requires statistical frameworks that simultaneously model these environmental and spatial drivers (Melles et al., 2009). Standard resource selection functions (RSFs) estimate habitat selection based on disproportionate use of available habitat, but often treat organismal habitat choices as spatially homogeneous and ignore residual spatial structure in occurrence data, leading to inflated parameter estimates and spurious inference (Northrup et al., 2022). Compounding this, RSFs often assign the spatial grain of analysis arbitrarily, potentially overlooking habitat features that exert their strongest influence at scales not considered by the study design (Johnson, 1980; McGarigal et al., 2016). Although integrated step-selection functions and autocorrelation-informed weighting approaches address related inferential problems, they require sequential movement data and remain unsuitable for point-occurrence datasets such as nest locations (Alston et al., 2023; Avgar et al., 2020). Incorporating spatially explicit variables derived from distance-based Moran's eigenvector maps (dbMEMs) addresses these limitations by partitioning variance in habitat selection among measured environmental features and spatial structure across multiple scales simultaneously (Borcard & Legendre, 2002; Dray et al., 2006). This decomposition provides unbiased measures of habitat selection independent of spatial autocorrelation, identifies patterns of scale-dependent habitat selection,

and quantifies residual spatial variance potentially attributable to social or philopatric processes operating independently of measured environmental gradients (Northrup et al., 2022). Spatial eigenvector mapping has shown promise in maximizing species distribution model fitting in non-equilibrium scenarios (De Marco et al., 2008), but this methodology has not been extended into behavioral habitat selection analyses.

Turtles serve as an ideal model system for applying this integrated framework because of the well-documented environmental and philopatric pressures influencing maternal nesting decisions. As ectothermic organisms that lack post-ovipositional parental care, turtle embryos depend entirely on the thermal (Butler et al., 2018; Roosenburg & Kelley, 1996) and hydric (Butler et al., 2004) conditions of the nest to dictate their growth, survival, and often sex. While females select specific locations using proximate cues like overhanging vegetation and elevation to optimize these environments, interpreting these choices is complicated by within-generation site fidelity and multi-generational natal philopatry. Although philopatry is adaptive in stable environments (Reinhold, 1998), it may become maladaptive if traditional nesting areas deteriorate due to environmental change (Carreras et al., 2018). Whether philopatry is adaptive is particularly critical in turtles because nesting females cannot use the fates of previous nests to inform future decisions, increasing the likelihood of a preference-performance mismatch leading to an ecological trap (Robertson & Hutto, 2006).

We implement a habitat selection analysis using a drone-derived mapping dataset to characterize the nesting decisions of the diamond-backed terrapin (*Malaclemys terrapin*; hereafter terrapin) across ecologically relevant spatial scales. This estuarine specialist of the United States nests on sandy beaches above the high-water line (Burger & Montevecchi, 1975), and populations exhibit clear latitudinal gradients in habitat selection: northern populations avoid

dense vegetation to maximize solar exposure (Feinberg & Burke, 2003), whereas southern populations select sites near vegetation to moderate extreme temperatures (Butler et al., 2018, 2022; Grosse et al., 2014). Although individual fidelity and philopatry are confirmed via mark-recapture and genetic techniques (Sheridan et al., 2010; Szerlag-Egger & McRobert, 2007), no studies have characterized these drivers within an integrated statistical framework alongside high-resolution environmental data. We hypothesize that females select nest sites based on structural habitat features that maximize embryo survival, predicting selection for vegetation at fine scales and elevation at broader scales, with hatching success positively correlated with selected features.

Methods

Study site

Grand Bay National Estuarine Research Reserve (GNDNERR; Fig. 1a) is a 7400-ha marine protected area within the greater Grand Bay estuary complex located along the Alabama-Mississippi coastline in the northern Gulf of Mexico (Jackson Co., MS, Mobile Co., AL). We conducted our study on Point aux Chenes beach, a 1.9-km beach located in GDNERR that supports the primary terrapin nesting population in the area (Heaton et al., 2022; Fig. 1b).

Nest surveys

We detected active and depredated terrapin nests throughout the study area from systematic visual encounter surveys conducted on foot during June-August 2023. Depredated nests were identified by the presence of an obvious excavated nest cavity and recently depredated eggshells. For all nests, we recorded locations using a Garmin GPSMAP 62 GPS unit (horizontal accuracy ±3m). For active nests, we determined average egg depth below the surface.

Eggs were replaced in the nest cavity in the orientation they were found, and nests were protected from nest predators using a 30×30×15cm cylindrical hardware cloth nest-protector secured in the ground with camping anchors. To assess patterns of nest mortality due to flooding, nests were left in place for approximately 6-7 weeks, which corresponds to approximately 90% of their incubation period. In the final two weeks of incubation the nests were excavated, egg status was noted for all eggs (e.g., intact, rotten, punctured by plant roots), and viable eggs were placed in artificial incubators until hatching.

UAV photogrammetry surveys

Drone-based surveys provide the high-resolution 3D data necessary to overcome the resolution limitations of satellite imagery for quantifying micro-environmental characteristics (Koger et al., 2023). We produced a 3D orthomosaic of nesting beach topography and vegetation by capturing high-resolution imagery using programmed flight routes with a Mavic Pro quadcopter (DJI: Shenzhen, China) equipped with a 12.35-megapixel camera. We conducted all flights between 29 June and 2 July 2023, within two hours of midday to standardize lighting and during periods of minimal wind to ensure high image quality (Supplement S1).

To ensure high horizontal accuracy and precise georeferencing from the UAV images, before all flights we distributed 20 ground control points (GCPs) at approximately 100m intervals throughout the study area. We used a Trimble R10 Real-Time Kinematic (RTK) Global Navigation Satellite System (GNSS) to record precise x, y, and z coordinates for each GCP centroid (horizontal accuracy: ±0.008m; vertical accuracy: ±0.015m). Finally, we projected all spatial data to the NAD 1983 StatePlane Mississippi East FIPS 2301 (EPSG:6506) coordinate system using meters as the unit of measure.

To create a 3D dense point cloud representing all topographic and vegetation surfaces of Point aux Chenes beach, we imported all 6343 UAV photos into Pix4Dmapper (v4.4.12, Pix4D Inc.) and used structure from motion (SfM) photogrammetry within Pix4Dmapper to estimate 3D structure of physical points in space photographed repeatedly from different positions (Supplement S1; Westoby et al., 2012). The result is a sub-centimeter-resolution (ground sampling distance=0.9cm/pixel), georeferenced 3D point cloud that can be directly analyzed or converted into a variety of geographic outputs, including orthorectified imagery and dense point clouds (Supplement S2).

Environmental variable extraction

To segment the complete point cloud into distinct topographic and vegetation surfaces, we used the qCANUPO plug-in (Brodu & Lague, 2012), a multi-scale dimensionality-based habitat classifier using linear discriminant analysis, available within CloudCompare (v2.13.2). The classifier was trained on manually labeled point cloud segments and validated against independent held-out data (Supplement S3; Table S1–S2). Post-classification point cloud processing, canopy height model derivation, marsh proximity calculation, and raster conversion are described in Supplement S4. The resulting five rasters—the digital terrain model (DTM), DTM-derived slope and aspect layers, canopy height model, and marsh proximity layer—were used for environmental variable extraction at actual nest sites and random available locations (Fig. 1c). We created a 1m radius buffer around each used and available location and extracted buffer-averaged terrain elevation, aspect, slope, vegetation height, and marsh proximity using the zonal statistics tool in QGIS. Aspect was decomposed into west-east and south-north components via sine and cosine transformation, with more positive values corresponding to more

easterly and northerly aspects, respectively. We also extracted vegetation height standard deviation within each buffer as an index of structural complexity (Torresani et al., 2020).

Spatial variable extraction

We accounted for spatial structure in terrapin nest locations using distance-based Moran's Eigenvector Maps (MEMs; Borcard & Legendre, 2002; Dray et al., 2006), an ordination technique that decomposes pairwise spatial relationships into scale-dependent patterns of spatial autocorrelation. We computed MEMs using the R package adespatial (v0.3.29) through a four-step ordination process (Dray, 2016). First, we constructed a distance matrix comprising all pairwise Euclidean distances among used and available locations. We then truncated this matrix using a threshold calculated as the length of the largest edge of a minimum spanning tree linking all points. Euclidean distances below this threshold were retained as neighbor connections, while distances exceeding the threshold were replaced with a value equal to four times the threshold. Finally, we inputted this truncated matrix into a principal coordinate analysis to yield $n-1$ orthogonal eigenvectors. This method allowed us to reconstruct spatial patterns across all scales while preserving the fine-scale structure propagated through the minimum spanning tree (Borcard & Legendre, 2002; Dray et al., 2006).

The eigenvalues of the resulting MEMs correspond to Moran's I coefficients of spatial autocorrelation (Moran, 1948). Because zero or negative eigenvalues do not accurately reflect spatial structure following distance matrix truncation, we restricted our analysis to MEMs with positive eigenvalues (Borcard & Legendre, 2002). To identify the specific scales at which terrapin nests exhibited non-random clustering, we performed forward selection of all MEMs using redundancy analysis (RDA) in the R (v4.5.2; R Core Team, 2025) package vegan (v.2.7.3; Oksanen et al., 2025). We modeled nest presence as a binary response variable against all MEM

predictors. This procedure identified 31 significant MEMs from the original 334. We grouped these 31 MEMs into three evenly-sized and ecologically meaningful scales based on natural breaks in a scree plot of Moran's I coefficients (Fig. S1). We estimated characteristic spatial scales by relating eigenvalue ranks to the range of pairwise point distances in the study area, bounded by the threshold distance (31.8m) and the maximum study extent (1927m). This yielded eleven broad-scale (1773 to 1927m), ten moderate-scale (1192 to 1773m), and ten fine-scale MEMs (202 to 1192m). We pooled eigenvector loadings within each scale group by summing the loadings to create three composite spatial variables. Because sites with similar loading values are spatially closer than expected by chance, these variables represent nesting clusters at each specific scale. Finally, we compiled these spatial variables with the extracted environmental predictors, including vegetation height and complexity, marsh proximity, elevation, slope, and aspect, into the final dataset for statistical analysis.

Statistical analyses

We modeled nest-site selection using a generalized linear model with a binomial distribution and logit link in R. The binary response variable distinguished known nests from available locations. To assess the scale-independent influence of microhabitat on the probability a location represented a known nest, we included terrain elevation, slope, aspect (linearized sine and cosine components), marsh proximity, vegetation height, and vegetation complexity as continuous predictors. We also included the three composite MEM spatial eigenvectors to identify habitat-independent spatial clustering. To evaluate whether selection for microhabitat varied across scales, we added interaction terms between each composite spatial variable and all environmental predictors. We standard deviation scaled and mean centered all continuous

predictors prior to analysis. To minimize overfitting, we performed backward stepwise variable selection. We then assessed the final model for collinearity using variance inflation factors.

Variance inflation factor analysis revealed high collinearity between mean canopy height and canopy height complexity (VIF>16). Given that vegetation structural complexity, as measured by canopy height variation, more directly reflects the nest microenvironment features hypothesized to influence oviposition site selection, we retained canopy height complexity and excluded canopy height from all subsequent analyses.

We evaluated hatching success using a generalized linear model (GLM) with a binomial distribution and logit link in R. Hatching success, the ratio of hatched to unhatched eggs per nest, was modeled as a function of the three composite MEM spatial eigenvectors, mean canopy height, canopy height variation, mean terrain elevation, marsh proximity, terrain aspect, slope, and mean egg depth. Due to the low sample size, we did not include any interaction terms. All continuous predictors were standard deviation scaled and centered.

We present all results as estimated marginal means to hold the influence of other variables constant (Lenth et al., 2025). While summary tables show model estimated coefficients on the linear predictor scale, the text and figures present results after back-transforming to the data scale. We report odds ratios (OR) with 95% confidence intervals, representing the change in nesting odds associated with a one standard deviation shift in microhabitat values.

Results

Nest site selection

We discovered 75 terrapin nests, including 22 active nests and 53 depredated nests (Fig. 1c.i-ii).Terrapins at GDNERR exhibit both scale-dependent and scale-independent selection of

several nest-site microhabitat features (Fig. 2; Table S3). These conclusions can be drawn by examining the relationship between our environmental and spatial MEM variables. Composite MEM loading values are unitless, habitat-independent indices of spatial autocorrelation in nest distributions at each scale, represented as spatially mapped, zero-centered values where clusters of locations with similar loading values characterize patterns of spatial autocorrelation at the corresponding MEM scale. Because MEM variables capture variance attributable to spatial structure, significant habitat-only terms in our analyses represent selection patterns consistent across the full study extent. Conversely, a significant MEM-by-habitat interaction indicates that the strength or direction of selection for a given feature varies spatially, implying some additional unmeasured factor modifies how that habitat feature predicts nesting probability across the study area.

Terrapin selection for vegetation complexity was conditional on broad-scale (1773 to 1927m) MEM loading values (Fig. 3b). In areas associated with negative broad-scale MEM loadings, a 0.07m (1 standard deviation) increase in vegetation complexity corresponded to 23.6% decreased odds of nesting (OR=0.76, 95% CI 0.52 to 1.13). However, in areas associated with positive broad-scale MEM loadings, the same increase in vegetation complexity corresponded to 52.2% increased odds of nesting (OR=1.52, 95% CI 1.13 to 2.06).

Selection for elevation was similarly conditional on broad-scale MEM loading values (Fig. 4b). In areas associated with negative broad-scale loadings, elevation had no detectable influence on nesting probability (OR=0.98, 95% CI 0.69 to 1.39), whereas in areas associated with positive broad-scale MEM loadings, a 0.28-m increase in elevation corresponded to 79.1% increased odds of nesting (OR=1.79, 95% CI 1.19 to 2.70).

Selection for terrain aspect along the west-east orientation was conditional on moderate-scale (1192 to 1773m) MEM loadings (Fig. 5b). In areas associated with negative moderate-scale MEM loadings, a 0.23-unit shift toward more easterly aspects corresponded to 34.8% decreased odds of nesting (OR=0.65, 95% CI 0.44 to 0.98), indicating preference for westerly aspects. This pattern reversed in areas associated with positive moderate-scale MEM loadings, where the same eastward shift corresponded to 40.9% increased odds of nesting (OR=1.41, 95% CI 0.96 to 2.07).

Finally, selection for proximity to the marsh edge was scale-independent, with an 8.68-m increase in distance from the marsh edge corresponding to 48.2% decreased odds of nesting across all MEM loading values (OR=0.52, 95% CI 0.37 to 0.73; Fig. S2).

Nest hatching success

We collected within-nest hatching success data from 22 terrapin nests during the 2023 nesting season. Average within-nest hatching success was 0.73 (SD=0.33; n=22). We found that hatching success was not significantly predicted by spatial structure at any scale (Table S4), indicating that the spatial patterning of nests does not itself predict offspring survival. Instead, hatching success was independently predicted by several microhabitat variables (Table S4). Vegetation complexity had a significant negative effect on hatching success ($\beta=-0.74$, SE=0.26, p=0.004; Fig. 3c), and terrain elevation also negatively predicted hatching success ($\beta=-1.39$, SE=0.38, $p < 0.001$; Fig. 4c). Easterly terrain was positively associated with hatching success ($\beta=0.81$, SE=0.28, p=0.004; Fig. 5c), while northerly terrain was negatively associated with egg survival ($\beta=-1.00$, SE=0.44, p=0.024; Fig. S3). Finally, slope had a positive effect on hatching success ($\beta=1.01$, SE=0.49, p=0.039; Fig. S4).

Discussion

We partitioned the relative influence of environmental quality and natal philopatry on nest site selection and hatching success in *M. terrapin*, thereby demonstrating for the first time methods to separate environmental, conspecific, and cultural sources of habitat selection from point count data. We hypothesized that females select nest sites based on vegetative and topographic features that maximize offspring survival, and our results provide partial support for this hypothesis. Maternal nest site selection was scale-dependent and multi-factorial: selection for vegetation complexity and elevation operated at broad spatial scales (1773 to 1927m), whereas selection for terrain aspect operated at moderate scales (1215 to 1659m). Critically, the strength and direction of selection for each habitat feature varied across space at the corresponding scale. For example, females in areas with negative moderate-scale MEM loadings preferentially nested on westerly aspects, whereas females in areas with positive moderate-scale MEM loadings preferentially nested on easterly terrain aspects, indicating that the direction of aspect selection reversed across the nesting beach according to spatial context. This spatial dependence is consistent with latent philopatric processes structuring nest distributions independently of measured environmental gradients. We also detected a preference-performance mismatch: females conditionally preferred areas of high elevation and vegetation complexity despite its negative association with hatching success, potentially signaling a philopatric ecological trap in which inherited site preferences have become decoupled from current habitat quality. To our knowledge, this is the first study to integrate resource selection functions with spatial eigenvector mapping to simultaneously quantify the relative contributions of scale-dependent environmental quality and latent philopatric processes to oviposition site selection and offspring survival. We argue that future application of this spatially-explicit

framework will promote unbiased estimates of the adaptive potential of both observed and latent maternal effects under sustained, directional environmental change.

Nest site selection

Significant interactions between environmental and spatial variables within our primary regression model indicate that patterns of terrapin nest-site selection are scale-dependent. Ecological theory suggests that habitat selection operates across nested spatiotemporal scales, each characterized by varying the overall extent or resolution of the dataset (Johnson, 1980; Wiens, 1976). However, this paradigm has led to reliance on arbitrary, a priori scale assignments that may not align with true organismal perception (Laforge et al., 2016; McGarigal et al., 2016). Unlike study extent and data resolution, which are explicitly researcher-defined, the spatial grain of habitat selection represents the scale at which environmental features are perceived and acted upon by the focal organism (Laforge et al., 2016; Mayor et al., 2009), and should therefore be determined analytically rather than assigned a priori (Isdell et al., 2015). Scale-optimization approaches address this by identifying the spatial structure in occurrence and environmental data before defining grain size (Levasseur et al., 2023; McGarigal et al., 2016).

Our findings show significant selection for vegetation complexity and elevation at broad spatial scales (1773 to 1927m), and for terrain aspect at moderate scales (1215 to 1659m). These patterns partially contradict theoretical expectations that the spatial scale of habitat selection should scale with the temporal frequency of environmental fluctuation (Mayor et al., 2009; Wiens, 1989). Fine-scale vegetation turnover through disturbance-succession cycles would predict selection for vegetation complexity at finer grains, whereas broad-scale topographic stability would predict selection for elevation and aspect at broader scales. However, coastal geomorphological dynamics may explain this discrepancy: large storm events can initiate

broad-scale patterns of vegetation disturbance and succession (Miller et al., 2010), whereas beach topography can shift at relatively fine spatial scales through interactions between beach width and localized sediment transport (Keijsers et al., 2014).

Overall patterns of nest site selection align with known terrapin preferences for close proximity to marsh boundaries and adjacent vegetation structure. However, we did not detect selection at fine spatial scales (<202m), contrary to substantial evidence of micro-scale associations between turtle nests and these habitat features (Janzen & Morjan, 2001; Kamel & Mrosovsky, 2005; Refsnider & Janzen, 2010; Roosenburg & Kelley, 1996; Wilson, 1998). We attribute this in part to the coarse minimum MEM grain resolvable from a single season of 75 nests, as more extensive within- and among-season sampling will likely be necessary to resolve selection processes operating below 200m.

Significant interactions between environmental and spatial variables also indicate that the strength and direction of habitat selection varies spatially across the nesting beach. Selection for vegetation complexity, elevation, and terrain aspect all varied with MEM loading values at their respective spatial scales, with selection strength weakening or reversing entirely between areas of negative and positive loadings (Fig. 3-5). Spatially varying selection coefficients have been documented as functional responses to shifting habitat availability across fragmented or heterogeneous landscapes and across distinct life stages (Holbrook et al., 2019; Matthiopoulos et al., 2011; Paton & Matthiopoulos, 2016). Yet our system encompasses a single terrapin life stage on a broadly homogeneous nesting beach, suggesting these explanations are insufficient and that alternative drivers warrant consideration (Avgar et al., 2020).

Previous work cautions that structured residual variation in distributional data may reflect unmeasured environmental covariates rather than true behavioral processes (Dormann et al.,

2007; Northrup et al., 2022). Several unmeasured factors could contribute to the spatially varying selection we observe. First, our vegetation classification distinguishes vegetation from topographic points but does not resolve taxonomic variation within vegetated areas. Butler et al. (2022) showed that terrapin nest locations in northern Florida are positively associated with a subset of plant species restricted to well-drained soils, suggesting vegetation community composition may matter independently of its structural complexity. Second, observed sand nuzzling and pilot hole digging at our site and in the literature suggest terrapins may also rely on thermal, chemical, or tactile cues not captured by our habitat maps (Morjan & Valenzuela, 2001). Finally, salt marsh structure adjacent to the nesting beach—excluded from our mapping reconstruction—may restrict access to certain beach areas, deflating the true availability of otherwise suitable sites and biasing selection estimates (Isdell et al., 2015).

Alternatively, residual spatial structure in our terrapin nesting distributions may reflect individual-level site fidelity coupled with high repeatability in nest site conditions. Terrapins and other turtles are capable of producing multiple clutches within a single nesting season, and repeatability of nest microenvironment preferences is well-documented in turtles (Janzen & Morjan, 2001; Kamel & Mrosovsky, 2005; Patrício et al., 2018). Moreover, the degree of nest site repeatability appears to increase with age (Delaney et al., 2020). Individual-level repeatable preferences for certain microenvironmental conditions may therefore explain the spatially dependent selection patterns we observe, and are consistent with demographic and population genetic evidence of matrilineal nest site philopatry in terrapins (Sheridan et al., 2010; Szerlag-Egger & McRobert, 2007). If philopatry was uncommon in this population and female offspring would consistently disperse to other nesting aggregations along the nesting beach, inherited microhabitat preferences would produce a more diffuse spatial signal, as returning

females would be distributed broadly across optimal habitat locations independent of their natal nest location. If philopatry is strong, however, repeatable preferences would sharpen this signal, resulting in spatially distinct nest clusters each reflecting a discrete matrilineal lineage exhibiting repeatable habitat choices. Future integration of genetic parentage assignment would allow further decomposition of these residual spatial signals into contributions from individual site fidelity, within-individual repeatability, and among-generation philopatry (Penttinen et al., 2026).

Nest hatching success

Patterns of nest site selection partially predict hatching success, revealing both preference-performance matches and mismatches that vary spatially across the beach. Selection for terrain aspect is spatially variable in direction, yet within each spatial grouping the preferred aspect aligns with its associated effect on hatching success, suggesting females make locally consistent assessments of microclimate conditions regardless of the direction of that preference (Refsnider & Janzen, 2010). By contrast, selection for vegetation complexity reveals a preference-performance mismatch: females generally prefer sites with high vegetation complexity despite its negative association with egg survival. This may reflect a documented trade-off in which dense vegetation moderates thermal extremes during incubation, while simultaneously promoting physical damage to eggs or hatchlings due to underlying root systems (Butler et al., 2018; Topping & Valenzuela, 2021). Spatial inconsistency in this mismatch may further reflect unmeasured variation in root architecture among plant types, such as clonal monocots versus eudicots, that is not captured by our above-ground structural measure of vegetation complexity.

Alternatively, this mismatch may represent a philopatric ecological trap in which cultural site fidelity perpetuates nest placement in locations where vegetation quality has shifted

(Robertson et al., 2013). This behavioral lag may prevent females from tracking contemporary optimal conditions as environments change (Robertson & Hutto, 2006). On dynamic coastal beaches, vegetation composition and structure can shift rapidly through successional processes, including the establishment and spread of invasive species (e.g., Vitex rotundifolia; Cousins et al., 2010). The reliability of historically inherited site preferences as indicators of current habitat quality is therefore expected to erode under climate-driven vegetation shifts and anthropogenic coastal development. Consequently, a population's capacity to respond adaptively depends on the relative strength of direct environmental assessment versus philopatric site fidelity. Long-term population monitoring combined with genetic parentage analysis will allow the degree of philopatric site fidelity to be estimated, and ultimately help determine whether philopatry constrains adaptive responses to shifting environmental conditions (Betts et al., 2008; Freedberg et al., 2005; Noble et al., 2018).

Conclusions

Oviposition site selection is a ubiquitous maternal effect with direct implications for offspring phenotypes and fitness, but how this process contributes to population-level responses to global change remains unclear due to the complex interplay of factors that drive it. Here, we examined the relative contributions of direct environmental assessment versus philopatric site fidelity on nest site selection in *M. terrapin* through the integration of resource selection functions, spatial eigenvector analyses, and 3D drone-based habitat mapping. Our analysis corroborates evidence that nest-site selection in turtles is a complex, multi-factorial process, and is the first to quantify residual spatial variance potentially attributable to latent patterns of site fidelity and philopatry. Preference-performance mismatches identified here further implicate philopatric inertia as a potential constraint on adaptive responses to shifting environmental

conditions. These conservation implications are especially acute for species, including many turtles, in which population persistence is disproportionately dependent on the sustained reproductive output of long-lived adult females to offset low juvenile survival and delayed maturation (Congdon et al., 1993; Crouse et al., 1987). Terrapin populations have suffered well-documented declines in adult female abundance range-wide due to commercial harvest, fisheries bycatch, and coastal development (Grosse et al., 2011; Seigel & Gibbons, 1995). However, current population viability analyses typically parameterize nest success from observed hatching rates without accounting for maladaptive site fidelity, potentially leading to systematic overestimates of reproductive contribution and underestimates of extinction risk under environmental change.

More broadly, spatial eigenvector analysis has emerged as a powerful and underutilized tool for simultaneously controlling for spatial autocorrelation, identifying relevant grain in spatiotemporal datasets, and quantifying latent spatial residuals consistent with social or philopatric processes. We argue this framework is widely applicable in any point-occurrence behavioral dataset (Hills & Thomason, 2003; Nicolaides et al., 2024) where latent environmental and social drivers of habitat selection remain unresolved.

References

Alston, J. M., Fleming, C. H., Kays, R., Streicher, J. P., Downs, C. T., Ramesh, T., Reineking, B., & Calabrese, J. M. (2023). Mitigating pseudoreplication and bias in resource selection functions with autocorrelation-informed weighting. *Methods in Ecology and Evolution*, *14*(2), 643–654. https://doi.org/10.1111/2041-210X.14025

Avgar, T., Betini, G. S., & Fryxell, J. M. (2020). Habitat selection patterns are density dependent under the ideal free distribution. *Journal of Animal Ecology*, *89*(12), 2777–2787. https://doi.org/10.1111/1365-2656.13352

Bernardo, J. (1996). Maternal effects in animal ecology. *American Zoologist*, *36*, 83–105.

Betts, M. G., Hadley, A. S., Rodenhouse, N., & Nocera, J. J. (2008). Social information trumps vegetation structure in breeding-site selection by a migrant songbird. *Proceedings of the Royal Society B: Biological Sciences*, *275*(1648), 2257–2263. https://doi.org/10.1098/rspb.2008.0217

Borcard, D., & Legendre, P. (2002). All-scale spatial analysis of ecological data by means of principal coordinates of neighbour matrices. *Ecological Modelling*, *153*(1–2), 51–68. https://doi.org/10.1016/S0304-3800(01)00501-4

Boström-Einarsson, L., Bonin, M. C., Munday, P. L., Jones, G. P., & Keith, S. A. (2025). Density dependent habitat selection in response to habitat loss in a coral reef fish. *Journal of Animal Ecology*, *94*(12), 2421–2430. https://doi.org/10.1111/1365-2656.70135

Brodu, N., & Lague, D. (2012). 3D terrestrial lidar data classification of complex natural scenes using a multi-scale dimensionality criterion: Applications in geomorphology. *ISPRS Journal of Photogrammetry and Remote Sensing*, *68*, 121–134. https://doi.org/10.1016/j.isprsjprs.2012.01.006

Burger, J., & Montevecchi, W. A. (1975). Nest Site Selection in the Terrapin Malaclemys terrapin. *Copeia*, *1975*(1), 113. https://doi.org/10.2307/1442413

Butler, J. A., Broadhurst, C., Green, M., & Mullin, Z. (2004). Nesting, nest predation and hatchling emergence of the Carolina diamondback terrapin, Malaclemys terrapin centrata, in northwestern Florida. *The American Midland Naturalist*, *152*(1), 145–155.

Butler, J. A., Burke, R. L., & Roosenburg, W. M. (2018). Reproductive behavior and ecology. In W. M. Roosenburg & V. S. Kennedy (Eds.), *Ecology and Conservation of the Diamond-backed Terrapin* (pp. 81–91). Johns Hopkins University Press.

Butler, J. A., Lambert, J. D., DeDeo, M., & Murphy, D. P. (2022). Population and Nesting Site Evidence for Diamondback Terrapins, Malaclemys terrapin, in Northeast Florida. *Frontiers in Ecology and Evolution*, *10*. https://doi.org/10.3389/fevo.2022.833199

Carreras, C., Pascual, M., Tomás, J., Marco, A., Hochscheid, S., Castillo, J. J., Gozalbes, P., Parga, M., Piovano, S., & Cardona, L. (2018). Sporadic nesting reveals long distance colonisation in the philopatric loggerhead sea turtle (Caretta caretta). *Scientific Reports*, *8*(1), 1435. https://doi.org/10.1038/s41598-018-19887-w

Congdon, J. D., Dunham, A. E., & Van Loben Sels, R. C. (1993). Delayed Sexual Maturity and Demographics of Blanding's Turtles (Emydoidea blandingii): Implications for Conservation and Management of Long-Lived Organisms. *Conservation Biology*, *7*(4), 826–833. https://doi.org/10.1046/j.1523-1739.1993.740826.x

Cousins, M. M., Briggs, J., Gresham, C., Whetstone, J., & Whitwell, T. (2010). Beach Vitex (Vitex rotundifolia): An Invasive Coastal Species. *Invasive Plant Science and Management*, *3*(3), 340–345. https://doi.org/10.1614/IPSM-D-09-00055.1

Crouse, D. T., Crowder, L. B., & Caswell, H. (1987). A Stage-Based Population Model for Loggerhead Sea Turtles and Implications for Conservation. *Ecology*, *68*(5), 1412–1423. https://doi.org/10.2307/1939225

De Marco, P., Diniz-Filho, J. A. F., & Bini, L. M. (2008). Spatial analysis improves species distribution modelling during range expansion. *Biology Letters*, *4*(5), 577–580. https://doi.org/10.1098/rsbl.2008.0210

Delaney, D. M., Hoekstra, L. A., & Janzen, F. J. (2020). Becoming creatures of habit: Among- and within-individual variation in nesting behaviour shift with age. *Journal of Evolutionary Biology*, *33*(11), 1614–1624. https://doi.org/10.1111/jeb.13701

Dormann, C., M. McPherson, J., B. Araújo, M., Bivand, R., Bolliger, J., Carl, G., G. Davies, R., Hirzel, A., Jetz, W., Daniel Kissling, W., Kühn, I., Ohlemüller, R., R. Peres-Neto, P., Reineking, B., Schröder, B., M. Schurr, F., & Wilson, R. (2007). Methods to account for spatial autocorrelation in the analysis of species distributional data: A review. *Ecography*, *30*(5), 609–628. https://doi.org/10.1111/j.2007.0906-7590.05171.x

Dray, S. (2016). *adespatial: Multivariate Multiscale Spatial Analysis* (p. 0.3-28) [Dataset]. https://doi.org/10.32614/CRAN.package.adespatial

Dray, S., Legendre, P., & Peres-Neto, P. R. (2006). Spatial modelling: A comprehensive framework for principal coordinate analysis of neighbour matrices (PCNM). *Ecological Modelling*, *196*(3), 483–493. https://doi.org/10.1016/j.ecolmodel.2006.02.015

Ellis, A. M. (2008). Incorporating density dependence into the oviposition preference–offspring performance hypothesis. *Journal of Animal Ecology*, *77*(2), 247–256. https://doi.org/10.1111/j.1365-2656.2007.01345.x

Feinberg, J. A., & Burke, R. L. (2003). Nesting ecology and predation of diamondback terrapins, Malaclemys terrapin, at Gateway National Recreation Area, New York. *Journal of Herpetology*, *37*(3), 517–526.

Freedberg, S., Ewert, M. A., Ridenhour, B. J., Neiman, M., & Nelson, C. E. (2005). Nesting fidelity and molecular evidence for natal homing in the freshwater turtle, Graptemys kohnii. *Proceedings of the Royal Society B: Biological Sciences*, *272*(1570), 1345–1350. https://doi.org/10.1098/rspb.2005.3080

Fretwell, S. D., & Lucas, H. L. (1969). On territorial behavior and other factors influencing habitat distribution in birds. *Acta Biotheoretica*, *19*(1), 16–36. https://doi.org/10.1007/BF01601953

Grosse, A. M., Crawford, B. A., Maerz, J. C., Buhlmann, K. A., Norton, T., Kaylor, M., & Tuberville, T. D. (2014). Effects of Vegetation Structure and Artificial Nesting Habitats on Hatchling Sex Determination and Nest Survival of Diamondback Terrapins. *Journal of Fish and Wildlife Management*, *6*(1), 19–28. https://doi.org/10.3996/082014-JFWM-063

Grosse, A. M., Maerz, J. C., Hepinstall‐Cymerman, J., & Dorcas, M. E. (2011). Effects of roads and crabbing pressures on diamondback terrapin populations in coastal Georgia. *The Journal of Wildlife Management*, *75*(4), 762–770. https://doi.org/10.1002/jwmg.104

Heaton, A. J., Archer, M. J., Mohrman, C., & Pitchford, J. L. (2022). Loss of Mississippi Diamondback Terrapin (Malaclemys terrapin pileata) Nesting Habitat in the Northern Gulf of Mexico. *Chelonian Conservation and Biology*, *21*(2), 272–276. https://doi.org/10.2744/CCB-1536.1

Hills, J. M., & Thomason, J. C. (2003). The ‘ghost of settlement past’ determines mortality and fecundity in the barnacle, Semibalanus balanoides. *Oikos*, *101*(3), 529–538. https://doi.org/10.1034/j.1600-0706.2003.12332.x

Holbrook, J. D., Olson, L. E., DeCesare, N. J., Hebblewhite, M., Squires, J. R., & Steenweg, R. (2019). Functional responses in habitat selection: Clarifying hypotheses and interpretations. *Ecological Applications: A Publication of the Ecological Society of America*, *29*(3), e01852. https://doi.org/10.1002/eap.1852

Isdell, R. E., Chambers, R. M., Bilkovic, D. M., & Leu, M. (2015). Effects of terrestrial–aquatic connectivity on an estuarine turtle. *Diversity and Distributions*, *21*(6), 643–653. https://doi.org/10.1111/ddi.12289

Janzen, F. J., & Morjan, C. L. (2001). Repeatability of microenvironment-specific nesting behaviour in a turtle with environmental sex determination. *Animal Behaviour*, *62*(1), 73–82.

Johnson, D. H. (1980). The comparison of usage and availability measurements for evaluating resource preference. *Ecology*, *61*, 65–71.

Kamel, S. J., & Mrosovsky, N. (2005). Repeatability of nesting preferences in the hawksbill sea turtle, Eretmochelys imbricata, and their fitness consequences. *Animal Behaviour*, *70*(4), 819–828. https://doi.org/10.1016/j.anbehav.2005.01.006

Keijsers, J. G. S., Poortinga, A., Riksen, M. J. P. M., & Maroulis, J. (2014). Spatio-Temporal Variability in Accretion and Erosion of Coastal Foredunes in the Netherlands: Regional Climate and Local Topography. *PLOS ONE*, *9*(3), e91115. https://doi.org/10.1371/journal.pone.0091115

Kirkpatrick, M., & Lande, R. (1989). The Evolution of Maternal Characters. *Evolution*, *43*(3), 485. https://doi.org/10.2307/2409054

Koger, B., Deshpande, A., Kerby, J. T., Graving, J. M., Costelloe, B. R., & Couzin, I. D. (2023). Quantifying the movement, behaviour and environmental context of group-living animals using drones and computer vision. *Journal of Animal Ecology*, *92*(7), 1357–1371. https://doi.org/10.1111/1365-2656.13904

Laforge, M. P., Brook, R. K., van Beest, F. M., Bayne, E. M., & McLoughlin, P. D. (2016). Grain-dependent functional responses in habitat selection. *Landscape Ecology*, *31*(4), 855–863. https://doi.org/10.1007/s10980-015-0298-x

Lenth, R. V., Banfai, B., Bolker, B., Buerkner, P., Giné-Vázquez, I., Herve, M., Jung, M., Love, J., Miguez, F., Piaskowski, J., Riebl, H., & Singmann, H. (2025). *emmeans: Estimated Marginal Means, aka Least-Squares Means* (Version 1.11.1) [Computer software]. https://cran.r-project.org/web/packages/emmeans/index.html

Levasseur, P., Prescott, R., Faherty, M., & Sutherland, C. (2023). Factors affecting spatiotemporal patterns of nest site selection and abundance in diamondback terrapins. *Ecology and Evolution*, *13*(3), e9866. https://doi.org/10.1002/ece3.9866

Matthiopoulos, J., Hebblewhite, M., Aarts, G., & Fieberg, J. (2011). Generalized functional responses for species distributions. *Ecology*, *92*(3), 583–589. https://doi.org/10.1890/10-0751.1

Mayor, S. J., Schneider, D. C., Schaefer, J. a., & Mahoney, S. P. (2009). Habitat Selection at Multiple Scales. *Ecoscience*, *16*(2), 238–247. https://doi.org/10.2980/16-2-3238

McGarigal, K., Wan, H. Y., Zeller, K. A., Timm, B. C., & Cushman, S. A. (2016). Multi-scale habitat selection modeling: A review and outlook. *Landscape Ecology*, *31*(6), 1161–1175. https://doi.org/10.1007/s10980-016-0374-x

Melles, S. J., Badzinski, D., Fortin, M.-J., Csillag, F., & Lindsay, K. (2009). Disentangling habitat and social drivers of nesting patterns in songbirds. *Landscape Ecology*, *24*(4), 519–531. https://doi.org/10.1007/s10980-009-9329-9

Miller, T. E., Gornish, E. S., & Buckley, H. L. (2010). Climate and coastal dune vegetation: Disturbance, recovery, and succession. *Plant Ecology*, *206*(1), 97–104. https://doi.org/10.1007/s11258-009-9626-z

Moran, P. A. P. (1948). The Interpretation of Statistical Maps. *Journal of the Royal Statistical Society. Series B (Methodological)*, *10*(2), 243–251.

Morjan, C. L., & Valenzuela, N. (2001). Is Ground-Nuzzling by Female Turtles Associated with Soil Surface Temperatures? *Journal of Herpetology*, *35*(4), 668–672. https://doi.org/10.2307/1565908

Mousseau, T., & Fox, C. (1998). The adaptive significance of maternal effects. *Trends in Ecology & Evolution*, *13*(10), 403–407. https://doi.org/10.1016/S0169-5347(98)01472-4

Nicolaides, S. G., Mostert, T. H. C., & McIntyre, T. (2024). Latrine site selection by African clawless otters, Aonyx capensis, and their behavior during latrine visitations. *Journal of Mammalogy*, *105*(1), 107–121. https://doi.org/10.1093/jmammal/gyad118

Noble, D. W. A., Stenhouse, V., & Schwanz, L. E. (2018). Developmental temperatures and phenotypic plasticity in reptiles: A systematic review and meta-analysis. *Biological Reviews*, *93*(1), 72–97. https://doi.org/10.1111/brv.12333

Northrup, J. M., Vander Wal, E., Bonar, M., Fieberg, J., Laforge, M. P., Leclerc, M., Prokopenko, C. M., & Gerber, B. D. (2022). Conceptual and methodological advances in habitat-selection modeling: Guidelines for ecology and evolution. *Ecological Applications*, *32*(1), e02470. https://doi.org/10.1002/eap.2470

Oksanen, J., Simpson, G. L., Blanchet, F. G., Kindt, R., Legendre, P., Minchin, P. R., O'Hara, R. B., Solymos, P., Stevens, M. H. H., Szoecs, E., Wagner, H., Barbour, M., Bedward, M., Bolker, B., Borcard, D., Borman, T., Carvalho, G., Chirico, M., Caceres, M. D., … Weedon, J. (2025). *vegan: Community Ecology Package*. https://CRAN.R-project.org/package=vegan

Paton, R. S., & Matthiopoulos, J. (2016). Defining the scale of habitat availability for models of habitat selection. *Ecology*, *97*(5), 1113–1122. https://doi.org/10.1890/14-2241.1

Patrício, A. R., Varela, M. R., Barbosa, C., Broderick, A. C., Ferreira Airaud, M. B., Godley, B. J., Regalla, A., Tilley, D., & Catry, P. (2018). Nest site selection repeatability of green turtles, Chelonia mydas, and consequences for offspring. *Animal Behaviour*, *139*, 91–102. https://doi.org/10.1016/j.anbehav.2018.03.006

Penttinen, I., Nebel, C., & Laaksonen, T. (2026). Habitat imprinting in breeding territory selection of a long-lived bird of prey. *Journal of Animal Ecology*, *95*(3), 470–481. https://doi.org/10.1111/1365-2656.70202

Refsnider, J. M., & Janzen, F. J. (2010). Putting Eggs in One Basket: Ecological and Evolutionary Hypotheses for Variation in Oviposition-Site Choice. *Annual Review of Ecology, Evolution, and Systematics*, *41*(1), 39–57. https://doi.org/10.1146/annurev-ecolsys-102209-144712

Reinhold, K. (1998). Nest-site philopatry and selection for environmental sex determination. *Evolutionary Ecology*, *12*(2), 245–250. https://doi.org/10.1023/A:1006591914859

Resetarits, W. J. (1996). Oviposition Site Choice and Life History Evolution. *American Zoologist*, *36*(January), 205–215.

Robertson, B. A., & Hutto, R. L. (2006). A framework for understanding ecological traps and an evaluation of existing evidence. *Ecology*, *87*(5), 1075–1085. https://doi.org/10.1890/0012-9658(2006)87%5B1075:affuet%5D2.0.co;2

Robertson, B. A., Rehage, J. S., & Sih, A. (2013). Ecological novelty and the emergence of evolutionary traps. *Trends in Ecology & Evolution*, *28*(9), 552–560. https://doi.org/10.1016/j.tree.2013.04.004

Roosenburg, W. M., & Kelley, K. C. (1996). The effect of egg size and incubation temperature on growth in the turtle, Malaclemys terrapin. *Journal of Herpetology*, *30*(2), 198–204.

Rudolf, V. H. W., & Rödel, M.-O. (2005). Oviposition site selection in a complex and variable environment: The role of habitat quality and conspecific cues. *Oecologia*, *142*(2), 316–325. https://doi.org/10.1007/s00442-004-1668-2

Rushing, C. S., Brandt Ryder, T., Valente, J. J., Scott Sillett, T., & Marra, P. P. (2021). Empirical tests of habitat selection theory reveal that conspecific density and patch quality, but not habitat amount, drive long-distance immigration in a wild bird. *Ecology Letters*, *24*(6), 1167–1177. https://doi.org/10.1111/ele.13729

Seigel, R. A., & Gibbons, J. W. (1995). Workshop on the ecology, status, and management of the diamondback terrapin (Malaclemys terrapin), Savannah River Ecology Laboratory, 2 August 1994; Final results and recommendations. *Chelonian Conservation and Biology*, *1*(3), 240–243.

Sheridan, C. M., Spotila, J. R., Bien, W. F., & Avery, H. W. (2010). Sex-biased dispersal and natal philopatry in the diamondback terrapin, Malaclemys terrapin. *Molecular Ecology*, *19*(24), 5497–5510. https://doi.org/10.1111/j.1365-294X.2010.04876.x

Szerlag-Egger, S., & McRobert, S. P. (2007). Northern Diamondback Terrapin Occurrence, Movement, and Nesting Activity Along a Salt Marsh Access Road. *Chelonian Conservation and Biology*, *6*(2), 295–301. https://doi.org/10.2744/1071-8443(2007)6%5B295:NDTOMA%5D2.0.CO;2

Topping, N. E., & Valenzuela, N. (2021). Turtle Nest-Site Choice, Anthropogenic Challenges, and Evolutionary Potential for Adaptation. *Frontiers in Ecology and Evolution*, *9*(December), 1–12. https://doi.org/10.3389/fevo.2021.808621

Weatherhead, P. J., & Forbes, M. R. L. (1994). Natal philopatry in passerine birds: Genetic or ecological influences? *Behavioral Ecology*, *5*(4), 426–433. https://doi.org/10.1093/beheco/5.4.426

Westoby, M. J., Brasington, J., Glasser, N. F., Hambrey, M. J., & Reynolds, J. M. (2012). 'Structure-from-Motion' photogrammetry: A low-cost, effective tool for geoscience applications. *Geomorphology*, *179*, 300–314. https://doi.org/10.1016/j.geomorph.2012.08.021

Wiens, J. A. (1976). Population Responses to Patchy Environments. *Annual Review of Ecology and Systematics*, *7*, 81–120.

Wiens, J. A. (1989). Spatial Scaling in Ecology. *Functional Ecology*, *3*(4), 385. https://doi.org/10.2307/2389612

Wilson, D. S. (1998). Nest-Site Selection: Microhabitat Variation and Its Effects on the Survival of Turtle Embryos. *Ecology*, *79*(6), 1884–1892. https://doi.org/10.1890/0012-9658(1998)079%5B1884:NSSMVA%5D2.0.CO;2

Figures

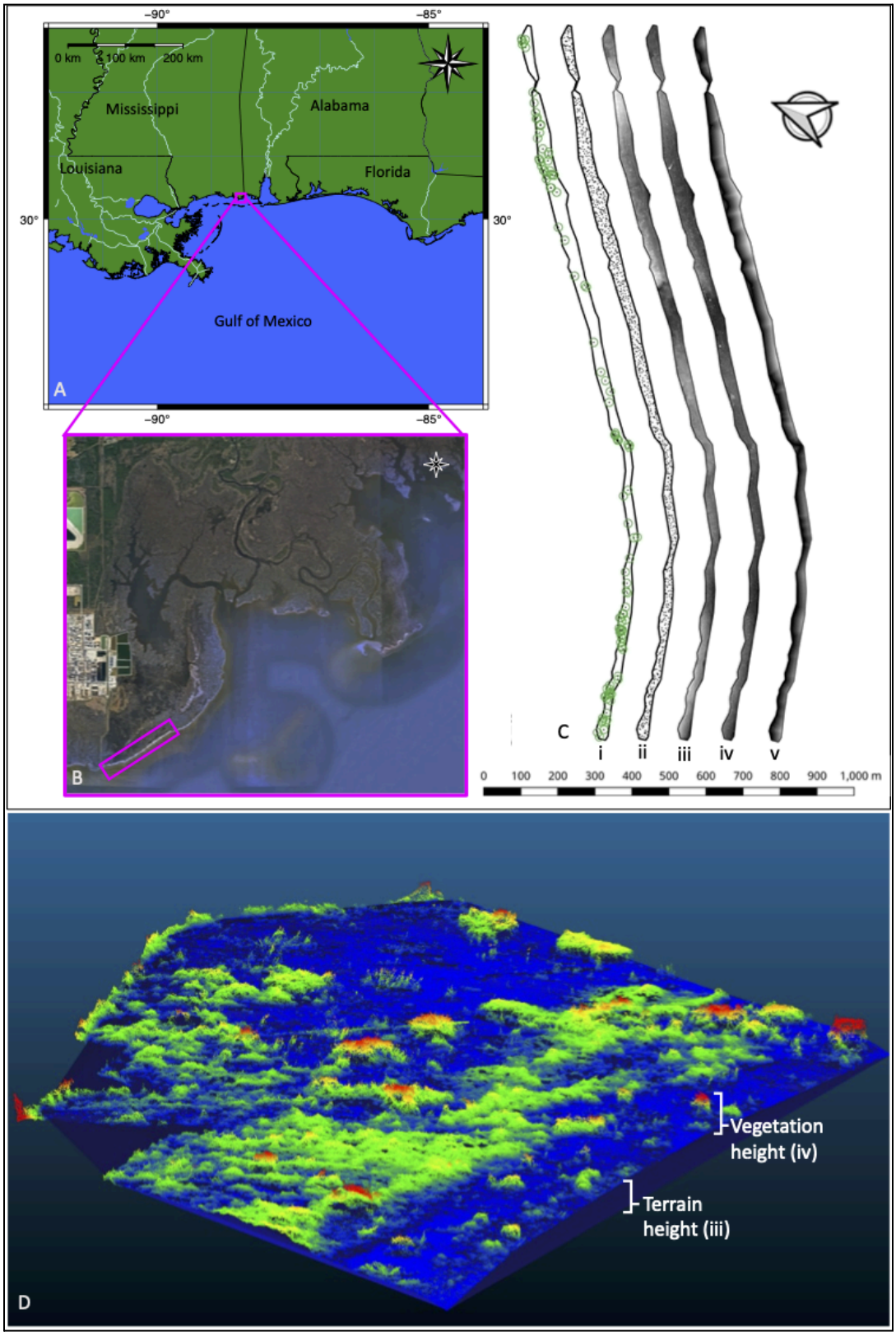
−90°
−85°
0 km
100 km
200 km
Mississippi
Alabama
Louisiana
Florida
30°
Gulf of Mexico
A
B
C
i
ii
iii
iv
v
0
100
200
300
400
500
600
700
800
900
1,000 m
Vegetation height (iv)
Terrain height (iii)
D

Figure 1. A) Geographic context and B) study extent along Point Aux Chenes beach at Grand Bay National Estuarine Research Reserve (image credit: Google Earth). C) GIS map layers showing i) diamond-backed terrapin (*Malaclemys terrapin*) nest locations (n=75), ii) random available locations (n=1194), iii) digital terrain model, iv) canopy height model, and v) marsh proximity. Increasingly white pixels (iii to v) correspond to increasing height and marsh distance values. D) 3D point cloud reconstruction illustrating derivation of vegetation and terrain height.

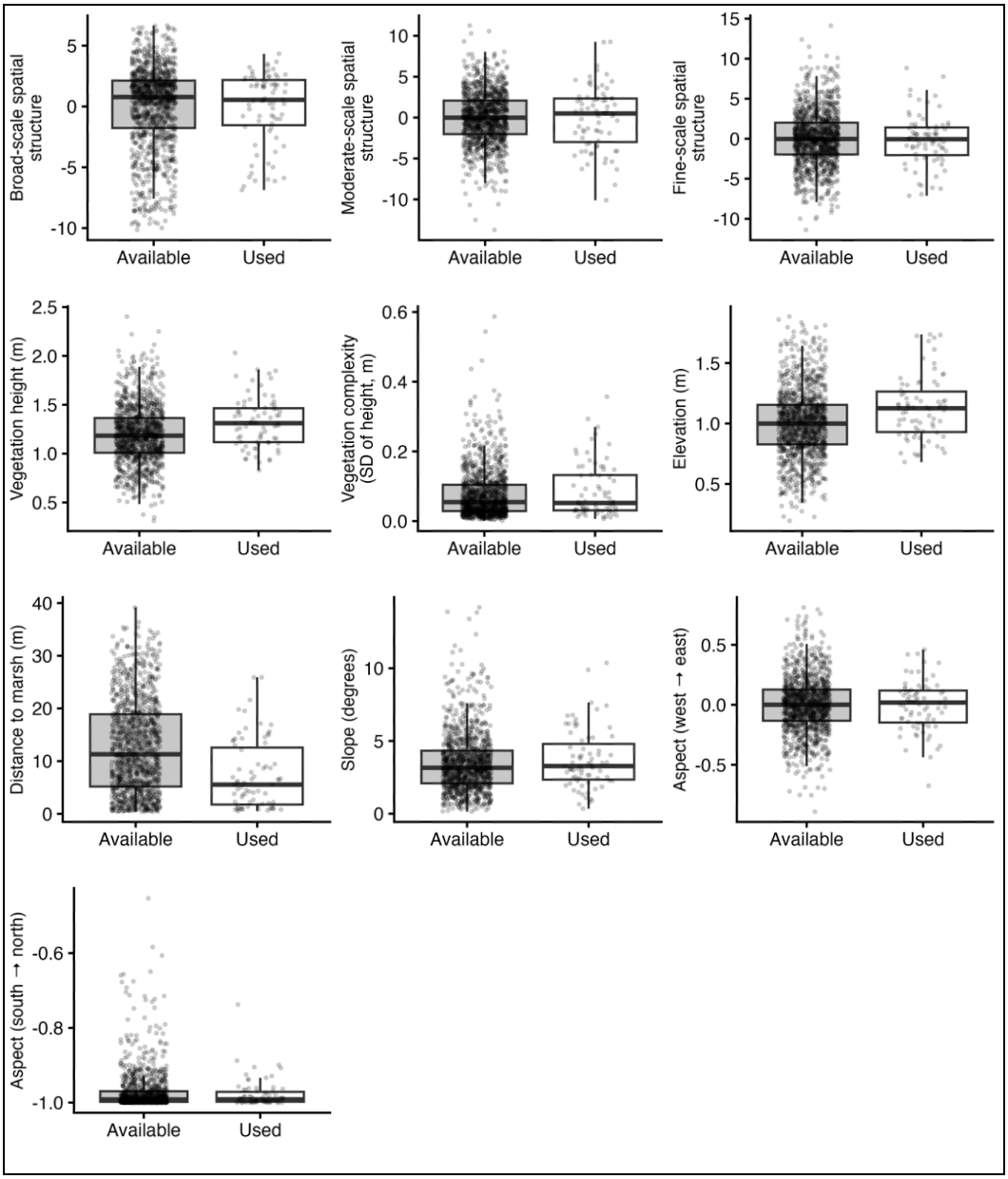

Figure 2. Spatial autocorrelation and microhabitat feature values at used (n=75) and available (n=1194) terrapin nest locations at Grand Bay NERR. Boxes show median and quartiles; whiskers extend to 1.5× the interquartile range.

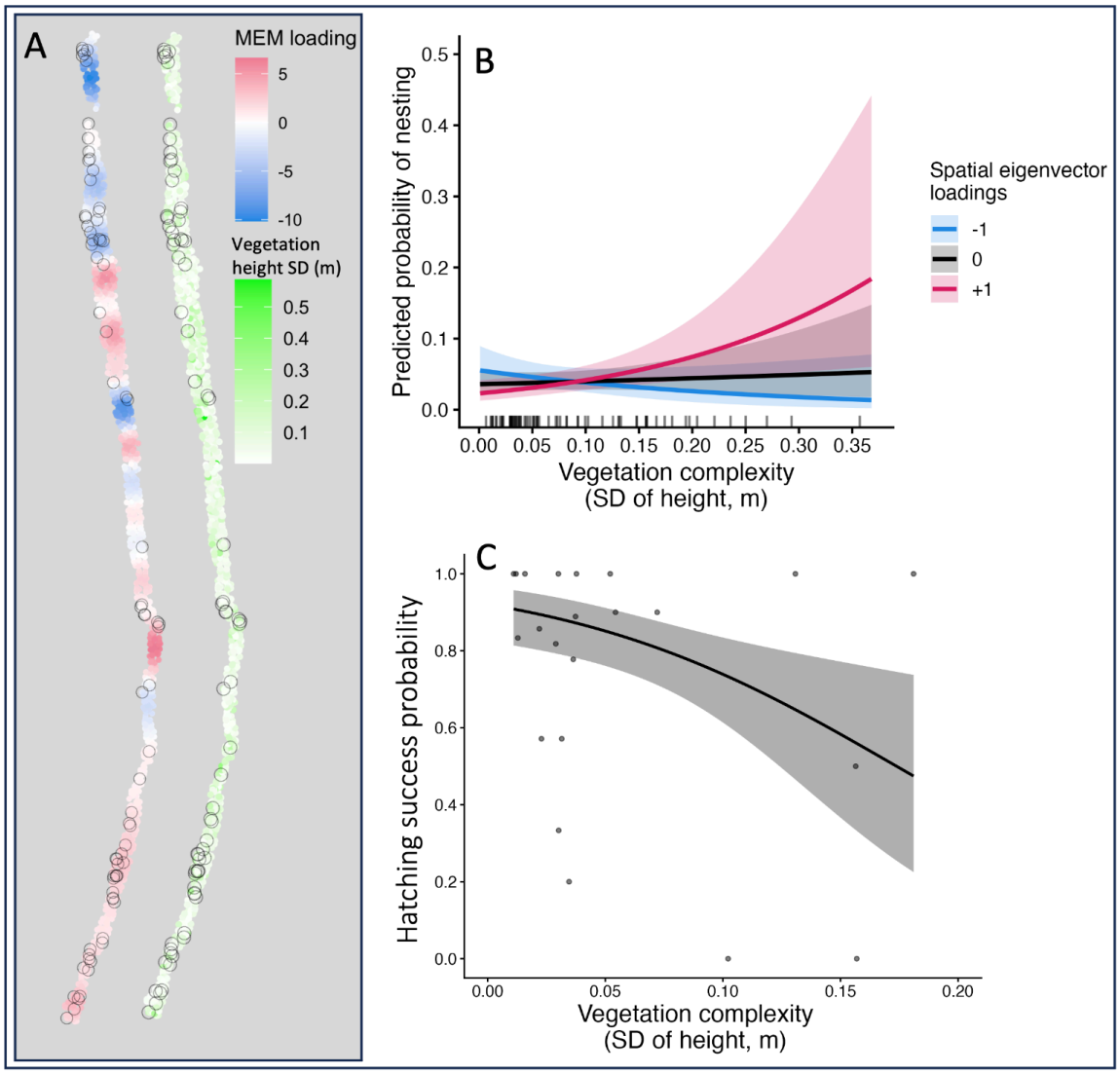

Figure 3. Influence of broad-scale (1773 to 1927m) vegetation complexity on nest site selection and hatching success in diamond-backed terrapins at Grand Bay NERR. A) Spatial distribution of broad-scale MEM loadings and vegetation complexity values; black circles indicate nest locations. B) Probability of nesting (n=75 used, 1194 available); black ticks indicate habitat values of used nests; red, black, and blue lines correspond to positive, zero, and negative moderate-scale MEM loadings, respectively. C) Hatching probability (n=22) as a function of vegetation complexity.

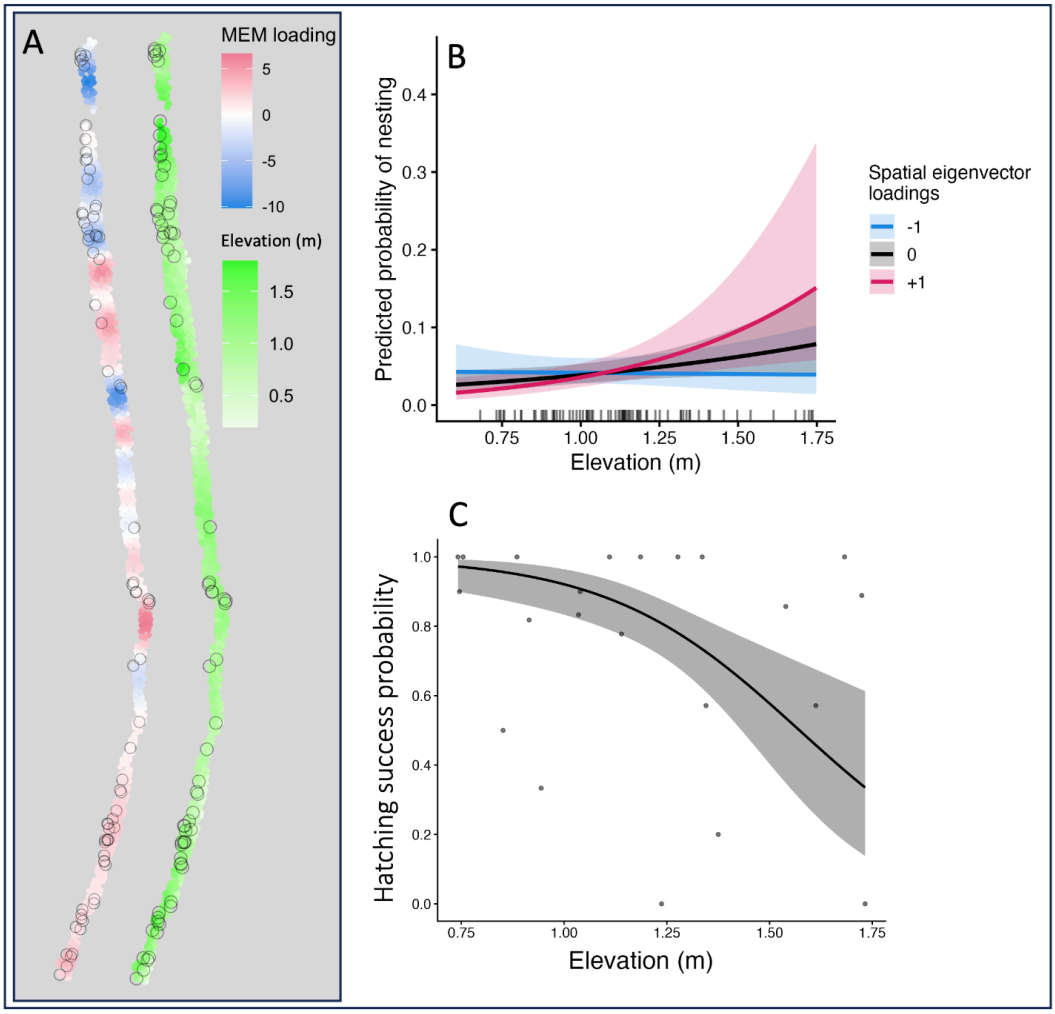

Figure 4. Influence of broad-scale (1773 to 1927m) terrain elevation on nest site selection and hatching success in diamond-backed terrapins at Grand Bay NERR. A) Spatial distribution of broad-scale MEM loadings and elevation values; black circles indicate nest locations. B) Probability of nesting (n=75 used, 1194 available); black ticks indicate habitat values of used nests; red, black, and blue lines correspond to positive, zero, and negative moderate-scale MEM loadings, respectively. C) Hatching probability (n=22) as a function of elevation.

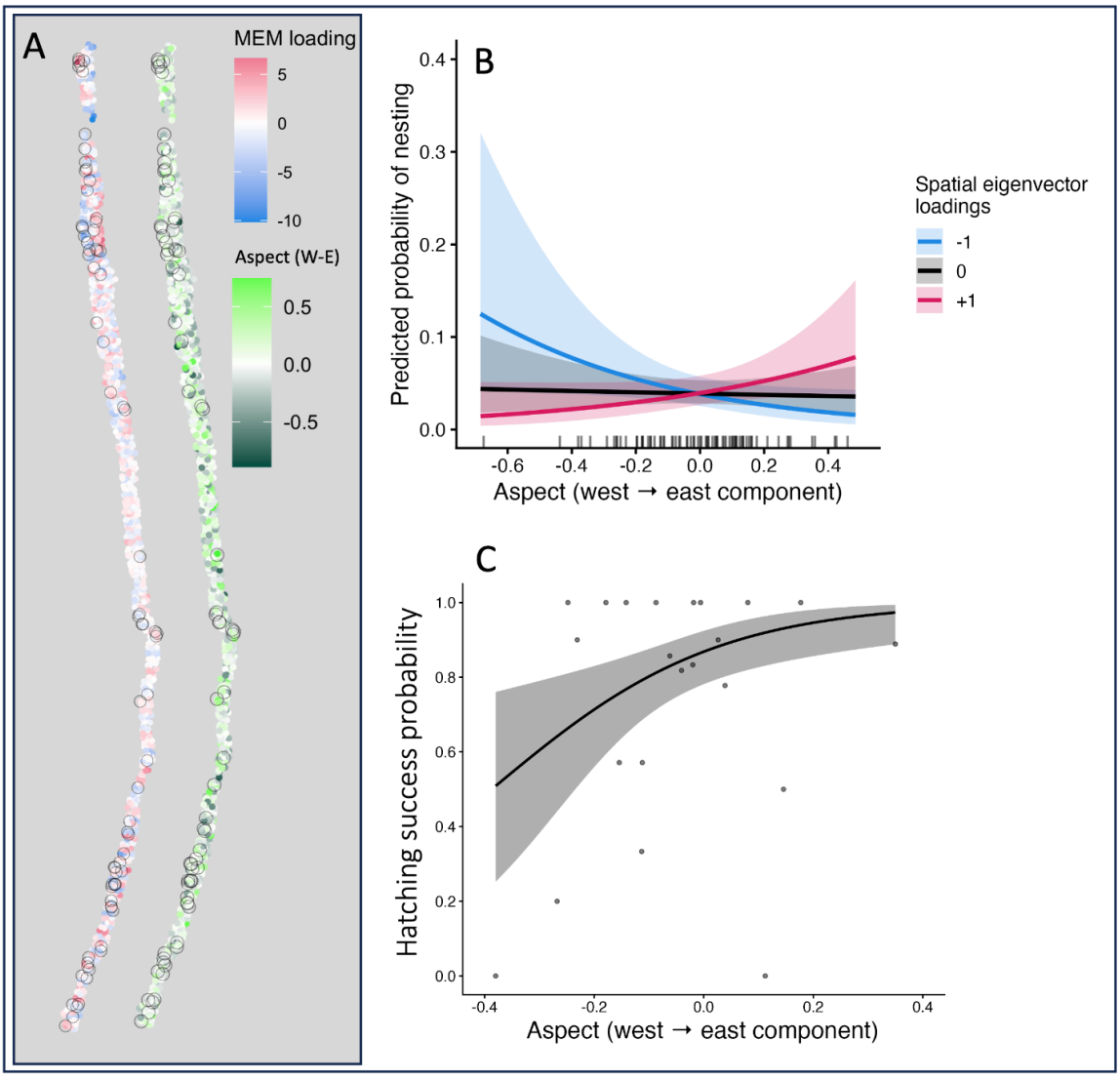

Figure 5. Influence of moderate-scale (1192 to 1773m) terrain aspect on nest site selection and hatching success in diamond-backed terrapins at Grand Bay NERR. A) Spatial distribution of moderate-scale MEM loadings and aspect values; black circles indicate nest locations. B) Probability of nesting (n=75 used, 1194 available); black ticks indicate habitat values of used nests; red, black, and blue lines correspond to positive, zero, and negative moderate-scale MEM loadings, respectively. C) hatching probability (n=22) as a function of terrain aspect.

Supplementary Materials

Table of Contents

Supplement S1. Map reconstruction.

We programmed consistent and repeatable flight routes using Drone Harmony software (v1.4.0). The UAV flew at a fixed altitude of 20m above ground level at a speed of 4m/s to minimize motion blur. We angled the camera 20 degrees above vertical and maintained 85% overlap of adjacent images to ensure 3D reconstruction accuracy. Final camera settings included automatic focus, f2.2 aperture, 1/800 shutter speed, and 100 ISO.

Ground control points (GCPs) were distributed at approximately 100m intervals, alternating placements between the high-tide line and the marsh edge to capture the full range of topographic variation. Fourteen GCPs were designated as independent checkpoints to validate final reconstruction accuracy. To integrate GCP data into the reconstruction, we used Pix4Dmapper's GCP manager to manually index all images containing GCPs and record the pixel Cartesian coordinates of each GCP centroid, georeferencing the point cloud with RTK-derived x, y, and z coordinates. GCPs were selectively enabled as either true ground control points, check points, or in one instance a manual tie point, depending on the computed position error and image projection error of the individual point, as well as the point’s position in the overall sequence to ensure a semiregular spacing of checkpoints (Supplement S2).

Quality Report

Generated with PIX4Dmapper version 4.10.1

Important: Click on the different icons for:

Help to analyze the results in the Quality Report

Additional information about the sections

Click here for additional tips to analyze the Quality Report

Summary

Project	GrandBayMap_UAB_AU
Processed	2026-04-28 22:05:35
Camera Model Name(s)	FC220_4.7_4000x3000 (RGB)
Average Ground Sampling Distance (GSD)	0.60 cm / 0.23 in
Area Covered	0.122 km^2 / 12.1541 ha / 0.05 sq. mi. / 30.0489 acres

Quality Check

Images	median of 39056 keypoints per image	✓
Dataset	6242 out of 6251 images calibrated (99%), 89 images disabled	✓
Camera Optimization	7.22% relative difference between initial and optimized internal camera parameters	⚠
Matching	median of 3991.28 matches per calibrated image	✓
Georeferencing	yes, 14 GCPs (14 3D), mean RMS error = 0.12 m	✗

Preview

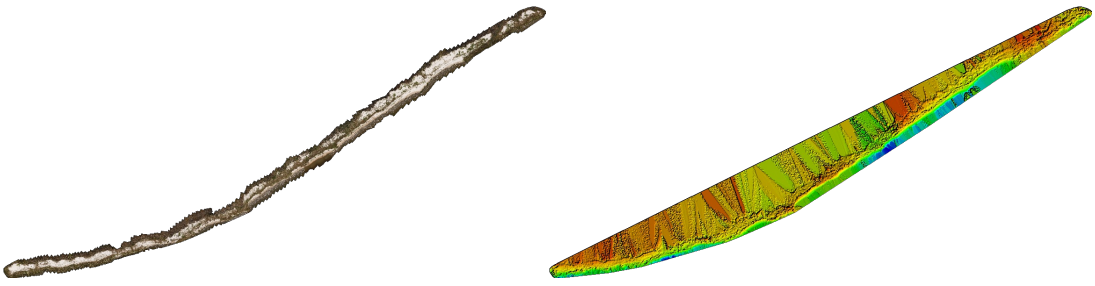

Figure 1: Orthomosaic and the corresponding sparse Digital Surface Model (DSM) before densification.

Calibration Details

Number of Calibrated Images	6242 out of 6340
Number of Geolocated Images	6340 out of 6340

Initial Image Positions

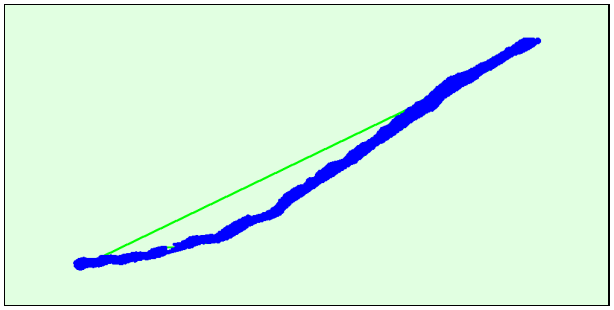

Figure 2: Top view of the initial image position. The green line follows the position of the images in time starting from the large blue dot.

Computed Image/GCPs/Manual Tie Points Positions

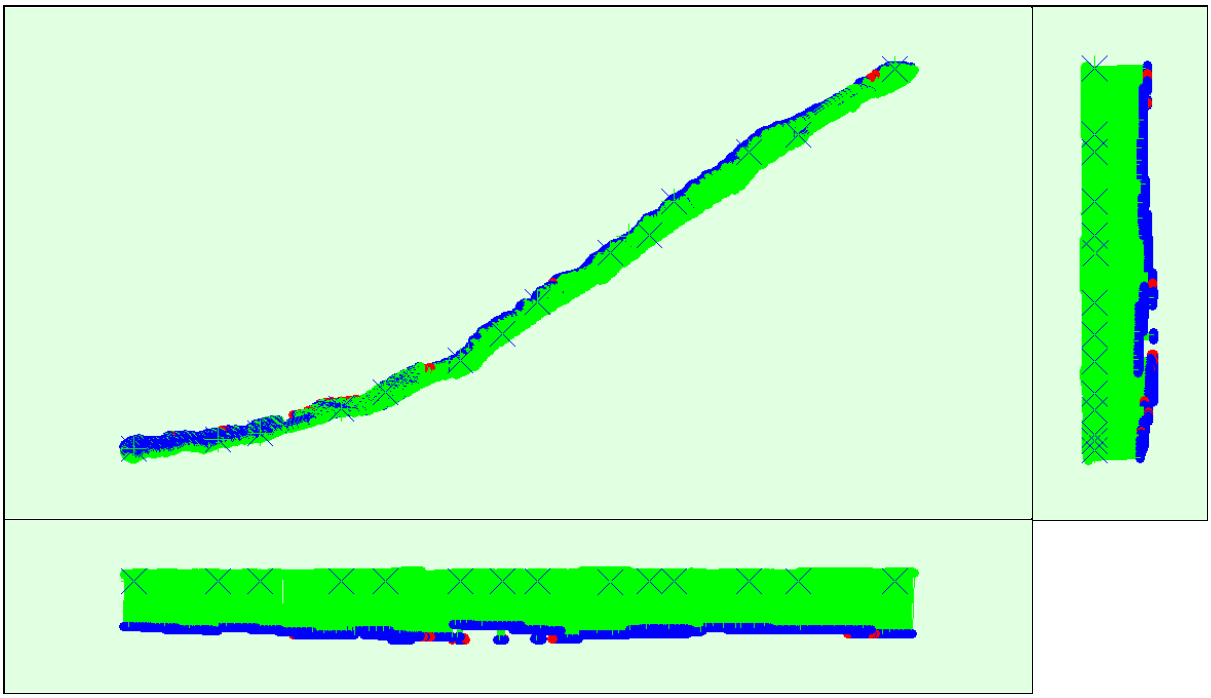

Uncertainty ellipses 10x magnified

Figure 3: Offset between initial (blue dots) and computed (green dots) image positions as well as the offset between the GCPs initial positions (blue crosses) and their computed positions (green crosses) in the top-view (XY plane), front-view (XZ plane), and side-view (YZ plane). Red dots indicate disabled or uncalibrated images. Dark green ellipses indicate the absolute position uncertainty of the bundle block adjustment result.

Absolute camera position and orientation uncertainties

	X [m]	Y [m]	Z [m]	Omega [degree]	Phi [degree]	Kappa [degree]	Camera Displacement X [m]	Camera Displacement Y [m]	Camera Displacement Z [m]
Mean	0.060	0.057	0.042	0.182	0.181	0.036	0.004	0.004	0.042
Sigma	0.028	0.029	0.009	0.114	0.098	0.020	0.002	0.002	0.019

Overlap

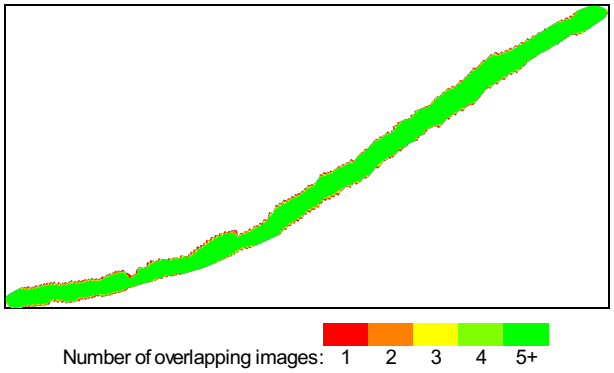

Figure 4: Number of overlapping images computed for each pixel of the orthomosaic.
Red and yellow areas indicate low overlap for which poor results may be generated. Green areas indicate an overlap of over 5 images for every pixel. Good quality results will be generated as long as the number of keypoint matches is also sufficient for these areas (see Figure 5 for keypoint matches).

Bundle Block Adjustment Details

Number of 2D Keypoint Observations for Bundle Block Adjustment	26631967
Number of 3D Points for Bundle Block Adjustment	9695331
Mean Reprojection Error [pixels]	0.208

Internal Camera Parameters

FC220_4.7_4000x3000 (RGB). Sensor Dimensions: 6.327 [mm] x 4.745 [mm]

EXIF ID: FC220_4.7_4000x3000

	Focal Length	Principal Point x	Principal Point y	R1	R2	R3	T1	T2
Initial Values	3073.410 [pixel] 4.861 [mm]	1917.790 [pixel] 3.033 [mm]	1485.800 [pixel] 2.350 [mm]	0.033	-0.086	0.078	0.000	-0.001
Optimized Values	2851.322 [pixel] 4.510 [mm]	1947.321 [pixel] 3.080 [mm]	1555.182 [pixel] 2.460 [mm]	0.028	-0.095	0.092	-0.001	0.001
Uncertainties (Sigma)	2.475 [pixel] 0.004 [mm]	0.154 [pixel] 0.000 [mm]	0.639 [pixel] 0.001 [mm]	0.000	0.000	0.001	0.000	0.000

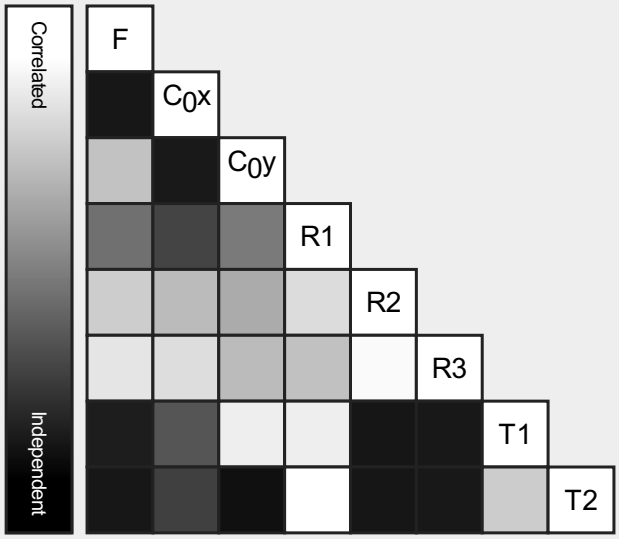

The correlation between camera internal parameters determined by the bundle adjustment. White indicates a full correlation between the parameters, ie. any change in one can be fully compensated by the other. Black indicates that the parameter is completely independent, and is not affected by other parameters.

The number of Automatic Tie Points (ATPs) per pixel, averaged over all images of the camera model, is color coded between black and white. White indicates that, on average, more than 16 ATPs have been extracted at the pixel location. Black indicates that, on average, 0 ATPs have been extracted at the pixel location. Click on the image to the see the average direction and magnitude of the re-projection error for each pixel. Note that the vectors are scaled for better visualization. The scale bar indicates the magnitude of 1 pixel error.

2D Keypoints Table

	Number of 2D Keypoints per Image	Number of Matched 2D Keypoints per Image
Median	39056	3991
Min	15934	62
Max	71220	13553
Mean	37877	4267

3D Points from 2D Keypoint Matches

	Number of 3D Points Observed
In 2 Images	6584996
In 3 Images	1657439
In 4 Images	648653
In 5 Images	314457
In 6 Images	169068
In 7 Images	95926
In 8 Images	59796
In 9 Images	39942
In 10 Images	27807
In 11 Images	20155
In 12 Images	14810
In 13 Images	11235
In 14 Images	8880
In 15 Images	6917
In 16 Images	5671
In 17 Images	4746
In 18 Images	3758
In 19 Images	3081
In 20 Images	2721
In 21 Images	2304
In 22 Images	1981
In 23 Images	1813
In 24 Images	1485
In 25 Images	1374
In 26 Images	1091
In 27 Images	943
In 28 Images	817
In 29 Images	670
In 30 Images	551
In 31 Images	432
In 32 Images	374
In 33 Images	255
In 34 Images	211
In 35 Images	196
In 36 Images	166
In 37 Images	96
In 38 Images	94
In 39 Images	75
In 40 Images	63

In 41 Images	56
In 42 Images	50
In 43 Images	28
In 44 Images	27
In 45 Images	24
In 46 Images	18
In 47 Images	12
In 48 Images	8
In 49 Images	12
In 50 Images	7
In 51 Images	12
In 52 Images	7
In 53 Images	5
In 54 Images	4
In 55 Images	8
In 56 Images	1
In 57 Images	2
In 58 Images	1

2D Keypoint Matches

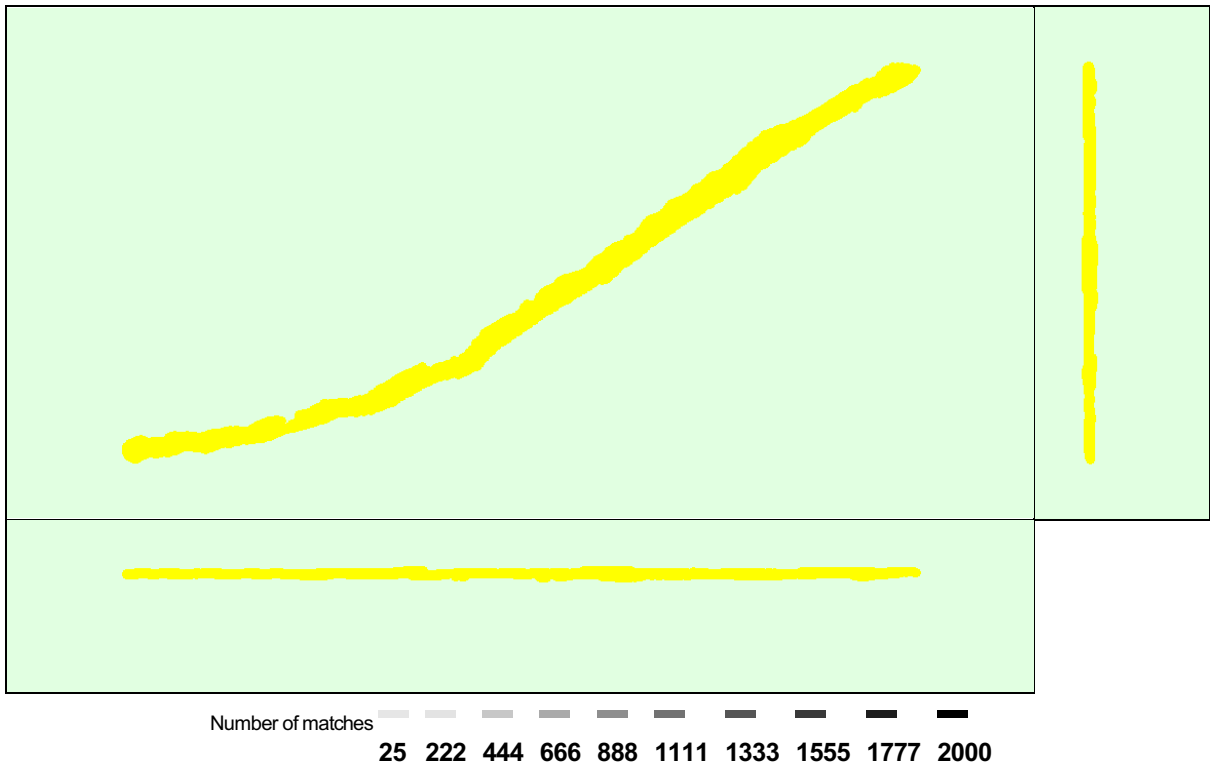

Figure 5: Computed image positions with links between matched images. The darkness of the links indicates the number of matched 2D keypoints between the images. Bright links indicate weak links and require manual tie points or more images.

Manual Tie Points

MTP Name	Projection Error [pixel]	Verified/Marked
mtp21	3.471	31 / 32
mtp22	1.305	9 / 17
mtp23	2.227	7 / 10
mtp24	2.264	22 / 28
mtp25	0.731	24 / 24
mtp26	3.642	15 / 15
mtp27	2.610	18 / 18
gcp_12	0.507	41 / 41

Projection errors for manual tie points.The last column counts the number of images where the manual tie point has been automatically verified vs. manually marked.

Geolocation Details

Ground Control Points

GCP Name	Accuracy XY/Z [m]	Error X [m]	Error Y [m]	Error Z [m]	Projection Error [pixel]	Verified/Marked
gcp_01 (3D)	0.100/ 0.150	0.006	-0.106	0.027	0.717	36 / 36
gcp_03 (3D)	0.100/ 0.150	-0.113	0.305	-0.193	0.680	31 / 31
gcp_04 (3D)	0.100/ 0.150	0.002	-0.106	0.003	0.611	25 / 25
gcp_06 (3D)	0.100/ 0.150	-0.017	-0.011	0.201	0.535	46 / 46
gcp_07 (3D)	0.100/ 0.150	0.015	-0.000	0.013	0.581	39 / 39
gcp_09 (3D)	0.100/ 0.150	0.117	0.004	-0.057	0.409	52 / 52
gcp_10 (3D)	0.100/ 0.150	-0.280	0.221	0.022	0.463	51 / 51
gcp_11 (3D)	0.100/ 0.150	0.099	-0.124	0.031	0.506	35 / 35
gcp_13 (3D)	0.100/ 0.150	0.082	-0.109	-0.066	0.698	42 / 42
gcp_14 (3D)	0.100/ 0.150	0.158	-0.245	0.152	0.486	44 / 44
gcp_15 (3D)	0.100/ 0.150	-0.140	0.257	-0.145	0.322	22 / 22
gcp_17 (3D)	0.100/ 0.150	0.032	0.034	0.031	0.664	34 / 34
gcp_18 (3D)	0.100/ 0.150	0.028	-0.095	-0.025	0.797	47 / 47
gcp_20 (3D)	0.100/ 0.150	0.010	-0.025	0.008	0.552	32 / 32
Mean [m]		0.000010	-0.000034	0.000049		
Sigma [m]		0.109735	0.153169	0.097724		
RMS Error [m]		0.109735	0.153169	0.097724		

0 out of 5 check points have been labeled as inaccurate.

Check Point Name	Accuracy XY/Z [m]	Error X [m]	Error Y [m]	Error Z [m]	Projection Error [pixel]	Verified/Marked
gcp_02		-0.0466	0.0694	-0.2138	0.6288	33 / 33
gcp_05		-0.7681	0.3677	0.1801	0.3094	32 / 32
gcp_08		-0.3737	0.1106	0.1613	0.6217	30 / 30
gcp_16		-0.4733	0.2861	0.3616	0.6975	36 / 36
gcp_19		0.0199	-0.1090	-0.4926	0.4328	44 / 44
Mean [m]		-0.328344	0.144958	-0.000655		
Sigma [m]		0.288851	0.167879	0.309048		
RMS Error [m]		0.437315	0.221802	0.309049		

Localisation accuracy per GCP and mean errors in the three coordinate directions. The last column counts the number of calibrated images where the GCP has been automatically verified vs. manually marked.

Absolute Geolocation Variance

Min Error [m]	Max Error [m]	Geolocation Error X [%]	Geolocation Error Y [%]	Geolocation Error Z [%]
-	-15.00	0.00	0.00	5.27
-15.00	-12.00	0.00	0.00	4.60
-12.00	-9.00	0.00	0.00	7.24
-9.00	-6.00	0.00	0.00	7.15
-6.00	-3.00	1.83	14.71	5.03
-3.00	0.00	42.21	31.32	11.45
0.00	3.00	55.74	47.34	18.46
3.00	6.00	0.22	6.57	17.56
6.00	9.00	0.00	0.06	13.73
9.00	12.00	0.00	0.00	7.61

12.00	15.00	0.00	0.00	1.91
15.00	-	0.00	0.00	0.00
Mean [m]		-2.514364	3.803511	-125.239835
Sigma [m]		1.795270	2.445044	7.775458
RMS Error [m]		3.089502	4.521608	125.480971

Min Error and Max Error represent geolocation error intervals between -1.5 and 1.5 times the maximum accuracy of all the images. Columns X, Y, Z show the percentage of images with geolocation errors within the predefined error intervals. The geolocation error is the difference between the initial and computed image positions. Note that the image geolocation errors do not correspond to the accuracy of the observed 3D points.

Geolocation Bias	X	Y	Z
Translation [m]	-2.514364	3.803511	-125.239835

Bias between image initial and computed geolocation given in output coordinate system.

Relative Geolocation Variance

Relative Geolocation Error	Images X [%]	Images Y [%]	Images Z [%]
[-1.00, 1.00]	100.00	98.21	80.05
[-2.00, 2.00]	100.00	100.00	99.26
[-3.00, 3.00]	100.00	100.00	100.00
Mean of Geolocation Accuracy [m]	5.000000	5.000000	10.000000
Sigma of Geolocation Accuracy [m]	0.000000	0.000000	0.000000

Images X, Y, Z represent the percentage of images with a relative geolocation error in X, Y, Z.

Geolocation Orientational Variance	RMS [degree]
Omega	1.337
Phi	1.300
Kappa	5.403

Geolocation RMS error of the orientation angles given by the difference between the initial and computed image orientation angles.

Rolling Shutter Statistics

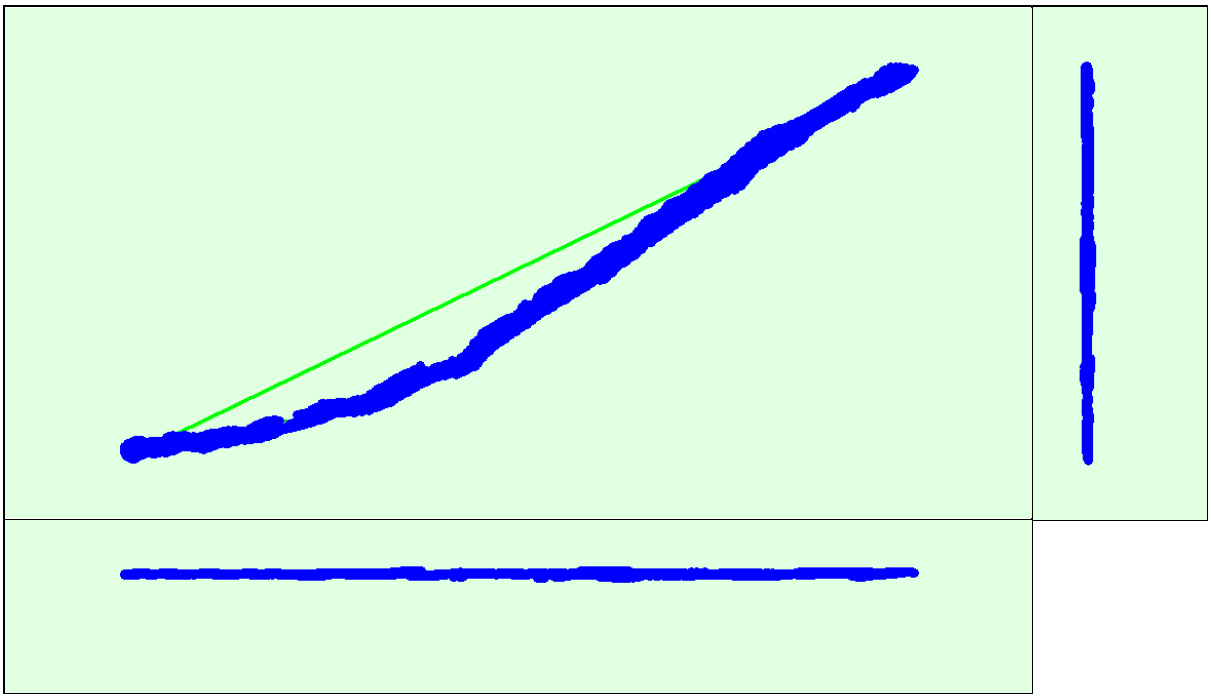

Figure 6: Camera movement estimated by the rolling shutter camera model. The green line follows the computed image positions. The blue dots represent the camera position at the start of the exposure. The blue lines represent the camera motion during the rolling shutter readout, re-scaled by a project dependant scaling factor for better visibility.

Median Camera Speed	2.9519 [m/s]
Median Camera Displacement During Sensor Readout)	0.2594 [m]
Median Rolling Shutter Readout Time	88.9749 [ms]

Initial Processing Details

System Information

Hardware	CPU: Intel(R) Core(TM) i7-7700K CPU @ 4.20GHz RAM: 32GB GPU: NVIDIA GeForce GTX 1070 (Driver: 32.0.15.6094)
Operating System	Windows 10 Pro, 64-bit

Coordinate Systems

Image Coordinate System	WGS 84 (EGM96 Geoid)
Ground Control Point (GCP) Coordinate System	WGS 84 / UTM zone 16N (EGM96 Geoid)
Output Coordinate System	WGS 84 / UTM zone 16N (EGM96 Geoid)

Processing Options

Detected Template	3D Maps
Keypoints Image Scale	Full, Image Scale: 1
Advanced: Matching Image Pairs	Aerial Grid or Corridor
Advanced: Matching Strategy	Use Geometrically Verified Matching: no
Advanced: Keypoint Extraction	Targeted Number of Keypoints: Automatic
Advanced: Calibration	Calibration Method: Standard Internal Parameters Optimization: All External Parameters Optimization: All Rematch: Auto, no

Point Cloud Densification details

Processing Options

Image Scale	multiscale, 1/2 (Half image size, Default)
Point Density	Optimal
Minimum Number of Matches	3
3D Textured Mesh Generation	yes
3D Textured Mesh Settings:	Resolution: Medium Resolution (default) Color Balancing: no
LOD	Generated: no
Advanced: 3D Textured Mesh Settings	Sample Density Divider: 1
Advanced: Image Groups	group1
Advanced: Use Processing Area	yes
Advanced: Use Annotations	yes
Time for Point Cloud Densification	1d:12h:06m:25s
Time for Point Cloud Classification	NA
Time for 3D Textured Mesh Generation	45m:14s

Results

Number of Processed Clusters	83
Number of Generated Tiles	8

Number of 3D Densified Points	350455421
Average Density (per m^3)	17392.4

DSM, Orthomosaic and Index Details

Processing Options

DSM and Orthomosaic Resolution	1 x GSD (0.596 [cm/pixel])
DSM Filters	Noise Filtering: yes Surface Smoothing: yes, Type: Sharp
Raster DSM	Generated: yes Method: Inverse Distance Weighting Merge Tiles: yes
Orthomosaic	Generated: yes Merge Tiles: yes GeoTIFF Without Transparency: no Google Maps Tiles and KML: no
Time for DSM Generation	05h:15m:44s
Time for Orthomosaic Generation	15h:00m:25s
Time for DTM Generation	00s
Time for Contour Lines Generation	00s
Time for Reflectance Map Generation	00s
Time for Index Map Generation	00s

Supplement S3: Habitat classifier development and validation.

qCANUPO uses machine-learning techniques to classify 3D points into pre-defined classes based on multi-scale dimensionality features computed at various spatial scales as characterized by a user-defined training dataset. A linear discriminant analysis is then used to train the classifier and apply it to the full dataset. To increase computational efficiency, we first used the spatial-subsampling tool in CloudCompare (v2.13.2) to thin the entire point cloud to a minimum nearest neighbor distance of 0.05m. We created a training dataset by using the scissor tool to manually select and classify 3D points representing two habitat classes: non-vegetated soil (e.g., bare sand) and vegetation (e.g., sparse or continuous expanses grasses, bushes, shrubs, and grasses > 0.1m in height). We classified these points within seven randomly selected 20m segments of the nesting beach, each containing both habitat classes in relative proportions representative of the surface area of the entire nesting beach. To create the classifier, we imported the manually labeled training dataset merged from five of the seven beach segments into the qCANUPO plug-in. The multi-scale dimensionality features were computed using scales ranging from 0.02m to 1.8m, with 0.2m steps. We reserved two of the seven beach segments (~30% of labeled points) as an independent test dataset to validate classifier performance. The trained habitat classifier we developed is available for validation and re-implementation as a prm-format parameter file.

The qCANUPO machine learning classifier was validated by comparing algorithm-assigned classifications (observed) against manually verified ground-truth labels (actual) for a subset of points from the study beach. The merged validation dataset comprised 447,716 points total (253,816 sand, 193,900 vegetation). Validation metrics were calculated on the subset of points with classification confidence > 0.75, retaining 373,043 points (83.3% of the

full dataset; 185,917 sand, 187,126 vegetation). Overall classification accuracy was 85.6% at this confidence threshold (Table S1-S2).

The asymmetry between sand precision (98.4%) and sand recall (72.3%) reflects a systematic boundary artifact rather than random misclassification error. Of the 51,572 sand points misclassified as vegetation, the large majority represent a known edge effect in point cloud classification where the vegetation class extends laterally onto effectively flat ground at stem bases. producing low-height returns with little structural significance for habitat analysis. In contrast, only 2,216 vegetation points were misclassified as sand, confirming that the vegetation class itself is captured with high fidelity (recall 98.8%).

Table S1. Performance metrics of point cloud classification for sand and vegetation surfaces.

Class	**Precision (%)[a]**	**Recall (%)[b]**	**F1Score[c]**
Sand	98.4	72.3	83.3
Vegetation	78.2	98.8	87.3

[a] *Precision: of all points classified as a given class, the proportion that were correctly classified (true positives / (true positives + false positives)).*
[b] *Recall: of all points belonging to a given class, the proportion that were correctly identified (true positives / (true positives + false negatives)).*
[c] *F1 Score: harmonic mean of precision and recall (2 × (precision × recall) / (precision + recall)), ranging 0–100.*

Table S2. Confusion matrix for point cloud classification of sand and vegetation surfaces.

	Reference: Sand	**Reference: Vegetation**
Classified: Sand	134345	2216
Classified: Vegetation	51572	184910

Supplement S4. Point cloud processing and environmental variable extraction.

Following classification, topographic and vegetation point clouds were processed separately to remove outliers and misclassified points. Both point clouds were trimmed to exclude high marsh and below sea-level points, and points with qCANUPO classification confidence values <75% were removed. For the topographic point cloud, we sequentially applied three noise reduction filters in CloudCompare: a plane-based noise filter, a nearest-neighbor-based statistical outlier removal (SOR) filter, and a cloth simulation filter (CSF; Zhang et al., 2016). For the vegetation point cloud, we applied a SOR filter. Gaps in the topographic point cloud created by vegetation removal were filled by converting the filtered cloud to a triangulated mesh using the Delaunay 2.5D best-fit plane method in CloudCompare, then resampling to generate a complete topographic surface.

Vegetation heights relative to ground level were quantified by calculating cloud-to-mesh distances in CloudCompare, with points returning negative height values removed as reconstruction noise, producing the final canopy height model. Marsh proximity was calculated using the cloud-to-primitive distance tool applied to a polyline representing the marsh boundary. All finalized point clouds were converted to raster format in QGIS, and terrain slope and aspect rasters were derived from the digital terrain model using the slope and aspect tools.

Supplement S5: Results figures and tables.

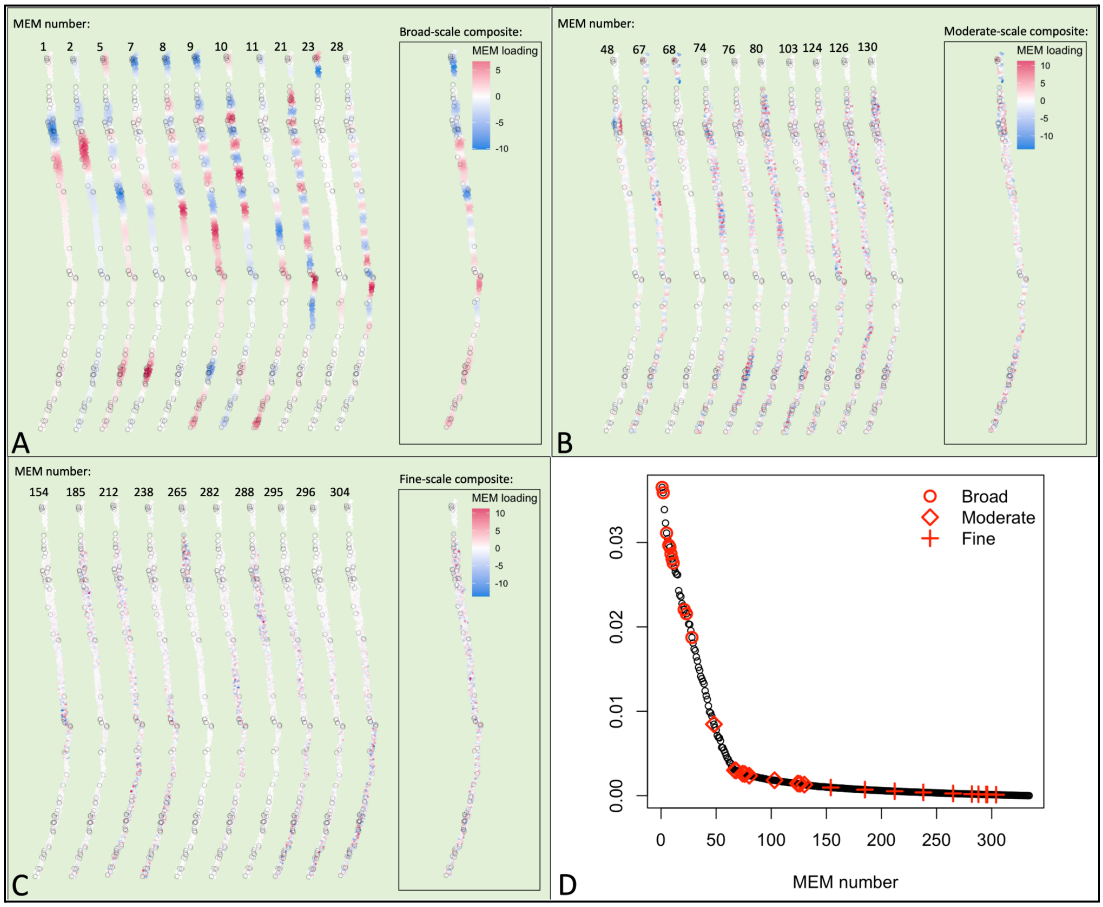

Figure S1. Visualization of Moran's eigenvector map (MEM) spatial variables.

A redundancy analysis was used to identify MEMs that describe patterns of spatial autocorrelation of terrapin nest locations at A) broad (n = 11 significant MEMs), B) moderate (n = 10 significant MEMs), and C) fine (n = 10 significant MEMs) spatial scales. Maps are composed of points representing all actual terrapin nests (n = 73) and available (n = 1194) sampling locations along the nesting beach. Point colors and relative opacities vary according to their loading value for each map's respective MEM, with bluer points having more negative loading, lower opacity/white points having low/zero loading values, and redder points having more positive loadings. Gray circles indicate actual nest locations. D) Scree plot depicting Moran's I coefficients for each of the 243 MEMs, ordered sequentially by eigenvalue rank. Red

points indicate the 31 significant MEMs used in the final analysis, with natural separations defining the composite grouping designations at broad-, moderate-, and fine microhabitat scale classes.

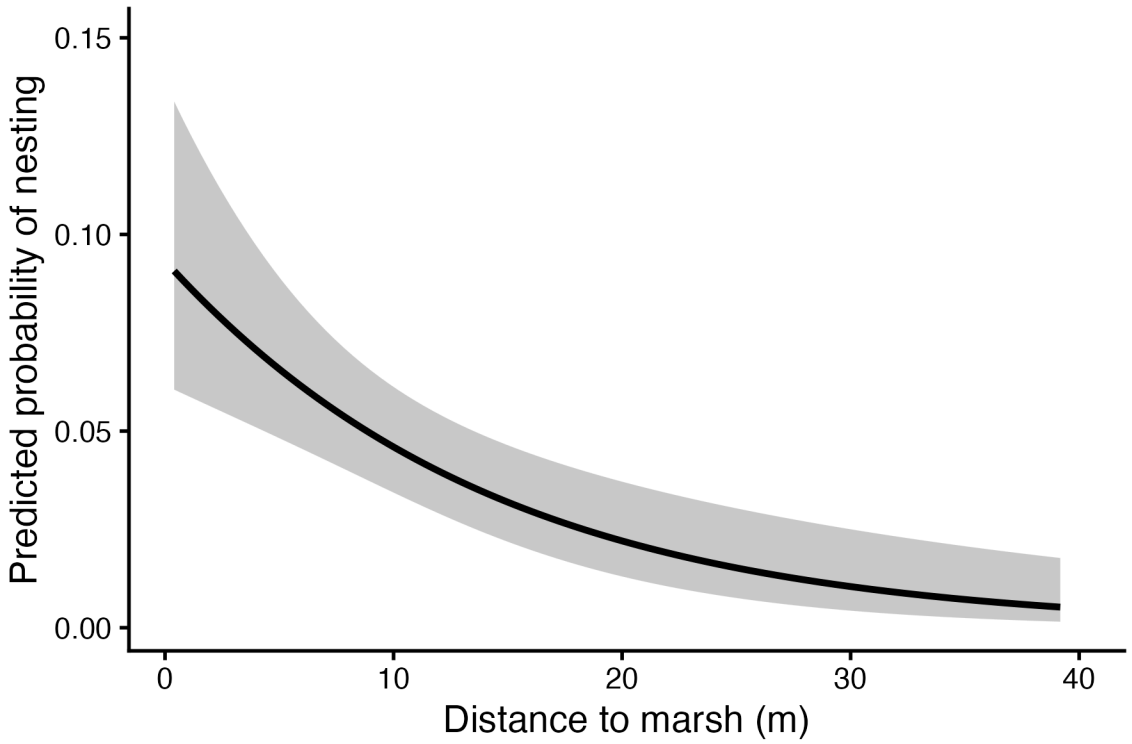

Figure S2. Marginal mean probability of nest site selection due to marsh proximity.

Predicted marginal mean probability (black line) and 95% confidence interval (grey shading) of nest site selection (n = 75 actual nests, 1194 available) as a function of marsh proximity, for diamond-backed terrapins (*Malaclemys terrapin*) at Grand Bay National Estuarine Research Reserve.

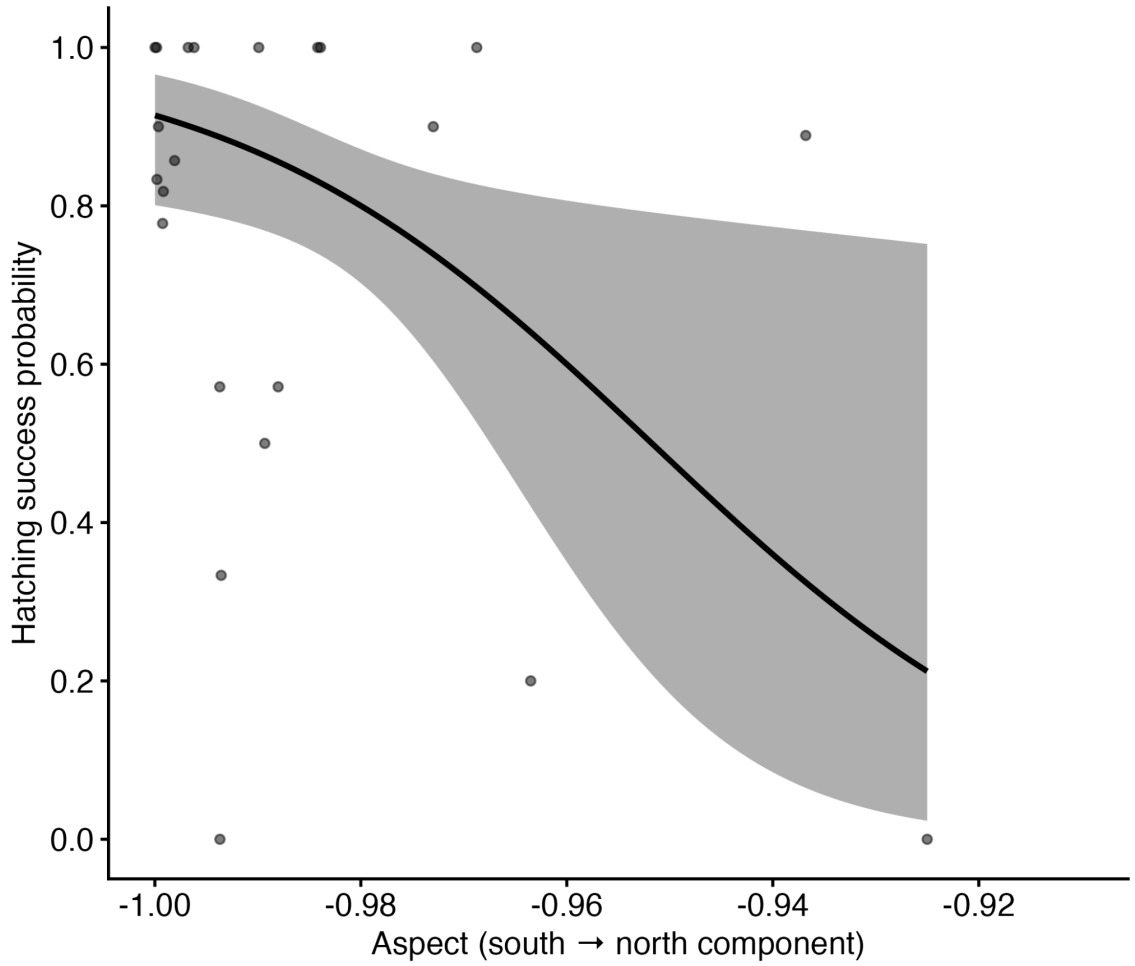

Figure S3. Marginal mean probability of hatching success due to terrain aspect (south-north).

Predicted marginal mean probability (black line) and 95% confidence interval (grey shading) of within-nest hatching success (n = 22) as a function of terrain aspect along the south-north axis, for diamond-backed terrapins (*Malaclemys terrapin*) at Grand Bay National Estuarine Research Reserve. Points represent observed proportions of hatching success of individual nests.

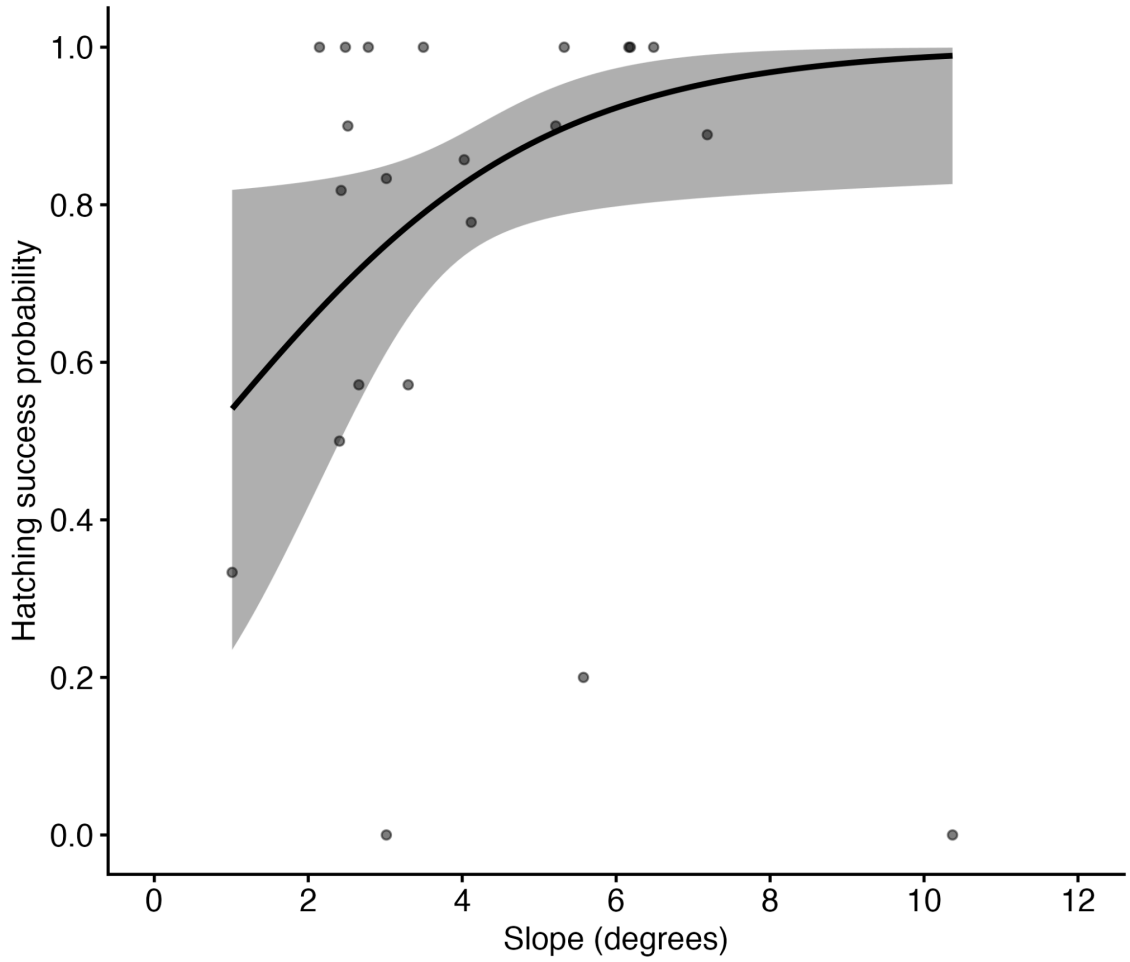

Figure S4. Marginal mean probability of hatching success due to terrain slope.

Predicted marginal mean probability (black line) and 95% confidence interval (grey shading) of within-nest hatching success (n = 22), as a function of terrain slope, for diamond-backed terrapins (*Malaclemys terrapin*) at Grand Bay National Estuarine Research Reserve. Points represent observed proportions of hatching success of individual nests.

Table S3. Binomial GLM summary for terrapin nest site selection.

Generalized linear model coefficients assessing the influence of environmental and spatial predictors on the probability of nest site selection in female diamond-backed terrapin (*Malaclemys terrapin*) at Grand Bay National Estuarine Research Reserve. Parameter estimates are presented on the log-odds (logit) scale, where positive values indicate increased probability of nesting and negative values indicate decreased probability. All continuous covariates were standard deviation scaled and mean centered prior to analysis.

Term	**Estimate**	**Std. Error**	**z value**	**p value**
(Intercept)	-3.20839	0.16908	-18.975	< 2e-16
Broad MEMs (1773 to 1927m)	-0.06976	0.12677	-0.55	0.582
Moderate MEMs (1192 to 1773m)	0.01658	0.12493	0.133	0.894
Fine MEMs (202 to 1192m)	-0.00131	0.12752	-0.01	0.992
Vegetation complexity (chm_stdev)	0.07561	0.1295	0.584	0.559
Elevation (dtm_mean)	0.27992	0.13589	2.06	0.039
Marsh distance (marsh_mean)	-0.65809	0.17283	-3.808	0.00014
Aspect sin (aspect_sin)	-0.04216	0.14403	-0.293	0.77
Aspect cos (aspect_cos)	-0.26794	0.18975	-1.412	0.158
Slope (slope_mean)	-0.06213	0.13182	-0.471	0.637
Broad MEMs x Vegetation complexity	0.34465	0.12318	2.798	0.005
Broad MEMs x Elevation	0.30277	0.14003	2.162	0.031
Moderate MEMs x Aspect sin	0.38529	0.14015	2.749	0.006
Moderate MEMs x Slope	-0.22478	0.13346	-1.684	0.092
Fine MEMs x Vegetation complexity	0.19917	0.12075	1.65	0.099

Table S4. Binomial GLM summary for terrapin hatching success.

Generalized linear model assessing influence of various environmental and Moran's eigenvector map (MEM) spatial predictors on the hatching probability of diamond-backed terrapin (*Malaclemys terrapin*) nests sampled at Grand Bay National Estuarine Research Reserve. Parameter estimates are presented on the log-odds (logit) scale, where positive values indicate increased probability of hatching success and negative values indicate decreased probability. All continuous covariates were standard deviation scaled and mean centered prior to analysis.

Term	Estimate	Std. Error	z value	p value
(Intercept)	1.65948	0.3135	5.293	<1.2e-07
Broad MEMs (1773 to 1927m)	0.1317	0.32994	0.399	0.69
Moderate MEMs (1192 to 1773m)	0.17853	0.3887	0.459	0.646
Fine MEMs (202 to 1192m)	-0.05524	0.26607	-0.208	0.836
Mean egg depth (avgEggDept)	0.60964	0.32691	1.865	0.062
Vegetation complexity (chm_stdev)	-0.73893	0.25602	-2.886	0.004
Elevation (dtm_mean)	-1.38824	0.3834	-3.621	0.00030
Marsh distance (marsh_mean)	-0.37771	0.42785	-0.883	0.377
Aspect sin (aspect_sin)	0.81298	0.27884	2.916	0.004
Aspect cos (aspect_cos)	-1.00388	0.44318	-2.265	0.024
Slope (slope_mean)	1.01125	0.49102	2.059	0.039